CORA Cork Open Research Archive
Cartlann Taighde Oscailte Chorcaí

Title	State-space modelling of the flight behaviour of a soaring bird provides new insights to migratory strategies
Authors	Pirotta, Enrico;Katzner, Todd;Miller, Tricia A.;Duerr, Adam E.;Braham, Melissa A.;New, Leslie
Publication date	2018-06-09
Original Citation	Pirotta, E., Katzner, T., Miller, T. A., Duerr, A. E., Braham, M. A. and New, L. (2018) 'State-space modelling of the flight behaviour of a soaring bird provides new insights to migratory strategies', Functional Ecology. doi:10.1111/1365-2435.13180
Type of publication	Article (peer-reviewed)
Link to publisher's version	10.1111/1365-2435.13180
Rights	© 2018, the Authors. Functional Ecology © British Ecological Society. Published by John Wiley & Sons Inc. This is the peer reviewed version of the following article: Pirotta, E., Katzner, T., Miller, T. A., Duerr, A. E., Braham, M. A. and New, L. (2018) 'State-space modelling of the flight behaviour of a soaring bird provides new insights to migratory strategies', Functional Ecology. doi:10.1111/1365-2435.13180, which has been published in final form at https://doi.org/10.1111/1365-2435.13180. This article may be used for non-commercial purposes in accordance with Wiley Terms and Conditions for Use of Self-Archived Versions.
Download date	2026-11-15 14:31:52
Item downloaded from	https://hdl.handle.net/10468/6599

UCC
University College Cork, Ireland
Coláiste na hOllscoile Corcaigh

State-space modelling of the flight behaviour of a soaring bird provides new insights to migratory strategies

Enrico Pirotta[a,b]*, Todd Katzner[c], Tricia A. Miller[d], Adam E. Duerr[e], Melissa A. Braham[f], and Leslie New[a]

[a] Department of Mathematics and Statistics, Washington State University, Vancouver, WA, USA

[b] School of Biological, Earth & Environmental, Sciences, University College Cork, Distillery Fields, North Mall, Cork, Ireland

[c] U.S. Geological Survey, Forest & Rangeland Ecosystem Science Center, Boise, ID, USA

[d] Conservation Science Global, West Cape May, NJ, USA

[e] Bloom Biological Inc., Santa Ana, CA, USA

[f] Division of Forestry & Natural Resources, West Virginia University, Morgantown, WV, USA

*Corresponding author: enrico.pirotta@wsu.edu

Abstract

1. Characterizing the spatiotemporal variation of animal behaviour can elucidate the way individuals interact with their environment and allocate energy. Increasing sophistication of tracking technologies paired with novel analytical approaches allows the characterisation of movement dynamics even when an individual is not directly observable.
2. In this study, high-resolution movement data collected via global positioning system (GPS) tracking in three dimensions were paired with topographical information and used in a Bayesian state-space model to describe the flight modes of migrating golden eagles (*Aquila chrysaetos*) in eastern North America.
3. Our model identified five functional behavioural states, two of which were previously undescribed variations on thermal soaring. The other states comprised gliding, perching and orographic soaring. States were discriminated by movement features in the horizontal (step length and turning angle) and vertical (change in altitude) planes, and by the association with ridgelines promoting wind deflection. Tracked eagles spent 2%, 31%, 38%, 9% and 20% of their day time in directed thermal soaring, gliding, convoluted thermal soaring, perching and orographic soaring, respectively. The analysis of the relative occurrence of these flight modes highlighted yearly, seasonal, age, individual and sex differences in flight strategy and performance. Particularly, less energy-efficient orographic soaring was more frequent in autumn, when thermals were less available. Adult birds were also better at optimising energy efficiency than sub-adults.
4. Our approach represents the first example of a state-space model for bird flight mode using altitude data in conjunction with horizontal locations, and is applicable to other

flying organisms where similar data are available. The ability to describe animal movements in a three-dimensional habitat is critical to advance our understanding of the functional processes driving animals' decisions.

Keywords: 3D states, GPS-GSM telemetry, hidden state model, Markov chain Monte Carlo, movement ecology, raptor, subsidised flight

Introduction

The way in which animals move in space and over time has important implications on their vital rates and, ultimately, their fitness and demography (Nathan et al., 2008). Different movement modes often require varying levels of energy expenditure and may reflect different environmental constraints (Shepard et al., 2013). Understanding movement dynamics and characterising the way in which they combine into functional bouts of activity can therefore help formulate hypotheses regarding movement drivers, environmental influences, and energetic and fitness implications of different behavioural strategies (Hays et al., 2016; Nathan et al., 2008).

Movement behaviour is difficult to observe directly for prolonged periods, especially for species that range over large distances and move through media that are mostly inaccessible to human observers (air or water). Recent advances in bio-logging technology allow tracking individuals over wide spatiotemporal ranges and in remote areas, opening windows on their life history at functionally relevant scales (Hays et al., 2016; Kays, Crofoot, Jetz, & Wikelski, 2015). Telemetry data collection was originally aimed at tracking an animal's geographical location. However, the proliferation of devices capable of collecting and storing information at fine temporal resolutions, combined with the refinement of statistical tools, means that these data can

also be used to infer the behavioural patterns of tagged animals (Jonsen et al., 2013; Langrock et al., 2012; McClintock, Russell, Matthiopoulos, & King, 2013; Patterson, Thomas, Wilcox, Ovaskainen, & Matthiopoulos, 2008).

While various techniques have been proposed for the classification of behaviour, hidden state models offer several advantages, particularly because they explicitly account for the intrinsic autocorrelation of movement data (Jonsen et al., 2013; Langrock et al., 2012; McClintock et al., 2012). These approaches assume that observed movement metrics arise from distributions that depend on a latent sequence of discrete behavioural states or modes (known as emission distributions), and are thus consistent with the often unobservable nature of behaviour. State assignment is directly informed by the data, which can guide behavioural classification, reveal unexpected patterns and thus lead to a new understanding of behaviour. State-space models, which constitute a class of hidden state models, also allow accounting for any measurement error associated with observed metrics (Jonsen et al., 2013; Patterson et al., 2008). This occurs because they are composed of a process model, capturing the underlying transition between states, and an observation model, describing the way in which data are generated, with error.

Most classic developments and applications of movement models have focused on the marine realm (e.g., marine mammals, seabirds, elasmobranchs or large teleosts, see references in Jonsen et al., 2013) or on terrestrial non-volant mammals (e.g. Morales, Haydon, Frair, Holsinger, & Fryxell, 2004). The main objective of these studies has been distinguishing between two behavioural modes: periods where an individual rapidly moves through unprofitable areas or travel corridors (transit mode), and periods where it explores an area in search of patchy food resources (resident mode) (Jonsen et al., 2013; Morales et al., 2004; Patterson et al., 2008).

Recently, important progress has been made in finer discrimination of behaviour by providing additional data streams to inform the models, characterizing, for example, attraction to specific locations (McClintock et al., 2012), central place foraging (Michelot et al., 2017; Pirotta, Edwards, New, & Thompson, 2018), diving (Bestley, Jonsen, Hindell, Harcourt, & Gales, 2015; Dean et al., 2013; Isojunno & Miller, 2015; Quick et al., 2017), and active foraging (Isojunno & Miller, 2015).

Few existing applications of hidden state models describe the behaviour of terrestrial birds (Leos-Barajas et al., 2017; Péron et al., 2017; Williams, Shepard, Duriez, & Lambertucci, 2015). For these species, characterising flight modes may be more relevant than distinguishing between transit and resident movement, because of the implications on their energy budget. Such characterisation requires either the use of additional sensors, like accelerometers, or the introduction of a third movement dimension (altitude), which is conceptually comparable to the use of depth when modelling diving behaviour of marine animals (Isojunno & Miller, 2015; Quick et al., 2017). Birds adopt different strategies to move through air, depending on their size, body structure, reasons for moving, and environmental and weather conditions (Duerr et al., 2015; Hedenstrom, 1993; Lanzone et al., 2012). Flapping flight is costly, and heavier species tend to soar (i.e. use air currents to support straight-winged flight) as a more efficient way to move over large distances (Hedenström & Alerstam, 1995). Broadly speaking, there are two predominant soaring modes in terrestrial birds. Thermal soaring is defined as the use of thermals (i.e. layers of warm air that rise from the earth forming updrafts) to gain altitude, followed by periods of gliding towards other thermals to continue their progression. Conversely, orographic soaring relies on horizontal winds deflected upwards by ridges, trees, hills and other structures (Duerr et al., 2015; Kerlinger, 1989).

In this study, a large telemetry dataset from golden eagles (*Aquila chrysaetos*) in eastern North America was used to develop a Bayesian state-space model describing the flight behaviour of soaring birds. These birds are from a small population of approximately 5,000 individuals migrating between the breeding grounds in Canada and a wintering range in the northern and central Appalachian Mountains and surrounding regions (Dennhardt, Duerr, Brandes, & Katzner, 2015; Katzner, Smith, et al., 2012). The population faces increasing pressure from wind power development in the southern part of its range and along its migratory route, which has sparked research on the factors influencing individuals' risk of colliding with turbines (Katzner, Brandes, et al., 2012; Miller et al., 2014). The choice of different flight modes by these birds changes their altitude, speed and updraft use and, although it is likely to contribute to collision risk, is rarely accounted for when predicting fatality rates (Barrios & Rodríguez, 2004; Klaassen, Strandberg, Hake, & Alerstam, 2008).

Golden eagles use both thermal and orographic soaring to maximise flight efficiency under different weather and environmental conditions (Duerr et al., 2012; Katzner et al., 2015; Lanzone et al., 2012). Therefore, they represent an ideal system for the development of a model to categorise flight modes, which could be easily applicable to other flying organisms. Below, the modelling framework is presented and utilized to characterise a high-resolution time series of golden eagle behaviour using location and altitude information collected via GPS, together with ancillary environmental data. The behavioural results are then analysed to investigate the activity budget of eagles belonging to different age and sex classes in different seasons, and to explore the functional mechanisms underpinning individual flight performance during migration.

Materials and methods

Data collection

We used existing golden eagle telemetry data collected between 2009 and 2016 (Duerr et al., 2012; Katzner et al., 2015; Miller et al., 2014). Eagles were captured and outfitted with CTT-1100 GPS-GSM telemetry systems (Cellular Tracking Technologies, LLC) attached as backpacks with Teflon™ ribbon (Bally Ribbon Mills in Bally, PA). Tags were programmed to record location and altitude above sea level (calculated as height above the geoid) every 30-60 seconds from sunrise to sunset. No locations were recorded at night. The GPS device measured instantaneous speed. If speed was less than 1 knot for 5 min, the unit switched to sampling data at 15-min intervals, thus conserving battery power and device memory when a bird was perching. Full details of the study area, deployment techniques, duty cycles, sampling regimes and permits are reported in Katzner et al. (2015) and Miller et al. (2014, 2016). For the current study, a total of 58 tracks were used, 48 of which were collected during the spring migration, and 10 in autumn (Fig. 1). Tagged eagles included juveniles (1st year of northbound migration, 8 tracks), sub-adults (2nd–4th year of migration, 22 tracks), and adults (>4th year of migration, 28 tracks). Nineteen tracks were from female individuals and 39 from males. Some individuals were tracked over multiple years (Table S1 in Supporting information).

Data processing

Fixes with a horizontal dilution of precision (an indication of 2D location quality; HDOP) > 10 and 2D fixes were removed to exclude any obvious error in GPS locations or altitudes. Vertical dilution of precision (VDOP) information was not available for the majority of the data. Due to

149 the sampling regime, there were gaps in the recorded tracks. Gaps in flight data could also have
150 occurred because of low battery voltage or the system's functionality. Furthermore, a unit could
151 not collect and send data simultaneously so, if a bird was in flight and connected to the Global
152 System for Mobile communications (GSM) network, GPS data were not collected. Therefore, to
153 reduce extrapolation over long unobserved periods, tracks from individual eagles were split into
154 separate segments whenever the interval between consecutive locations was greater than 5
155 minutes. Segments shorter than 10 minutes were excluded from further analysis to avoid biasing
156 the probabilities regulating the temporal sequence of states (see below). Because hidden state
157 models require a regular sampling unit, location and altitude data were linearly interpolated in R
158 with custom code to a constant one-minute temporal resolution (R Development Core Team,
159 2016). In alternative to using the interpolated values of the response variables over remaining
160 short ($\leq$ 5 min) unobserved periods in the data, the model can be formulated to estimate the value
161 of missing observations. Results of this reformulation are shown in Appendix S3.

162 At each minute, t, four variables were derived to characterise eagle behaviour (Table S2). The
163 use of these variables for describing the behaviour of soaring birds was supported by previous
164 studies (Katzner et al., 2015). Three of the four were derived from the GPS data: step length x_t
165 (the distance between location at t and location at $t + 1$, in meters), turning angle θ_t (the angle
166 between the step from $t - 1$ to t and the step from t to $t + 1$, in radians) and altitude above sea
167 level a_t (recorded by the GPS device, in meters). The fourth variable was hierarchical slope
168 position (HSP, as defined by Murphy, Evans & Storfer 2010), a metric of topographic
169 morphology used to quantify exposure and identify ridges. HSP was computed using package
170 spatialEco in R (Evans, 2017) and based on ground elevation data obtained from the Global
171 Multi-resolution Terrain Elevation Data 2010 at 30-arc-second spatial resolution (data available

from the U.S. Geological Survey: https://earthexplorer.usgs.gov/). A value of HSP, h_t, was extracted for the surface below each eagle location at time t. These four variables constituted the vector of behavioural observations $\mathbf{y}_t$. Because the calculation of the turning angle θ_t requires three consecutive locations, the first and last locations of each segment were discarded.

We assumed that the error around GPS locations was negligible (Morales et al., 2004). This was supported by the low mean HDOP associated with retained GPS fixes (mean = 1.9; STD = 1.2), corresponding to location errors in the order of a few meters. Particularly, the standard deviation of the position can be approximated by multiplying HDOP by the measurement standard deviation of the GPS device (Poessel, Duerr, Hall, Braham, & Katzner, 2018), which was 3 m for the devices used in this study (resulting in a standard deviation of 30 m when HDOP = 10). Considering the distribution of step lengths for tagged animals (mean = 540 m; STD = 398 m), this error was deemed irrelevant for our application. We used the published accuracy of the device in the third dimension to inform the error around altitude measurements in a state-space modelling framework (see details below; Lanzone et al., 2012).

We tested the use of altitude above ground level for the vertical dimension, but found models with this variable to perform much worse than those with altitude above sea level. This was possibly due to error propagation (Péron et al., 2017) or to the fact that altitude above ground becomes difficult to interpret over steeply changing slopes, such as the ones used during orographic flight (Katzner et al., 2015).

Model structure

We developed a Bayesian state-space model to estimate the time series of latent behavioural states, s_t, of tagged individuals, together with the state-specific parameters of the emission

194 distributions for the observations $\mathbf{y}_t$. The process component of the model described the
195 transition between the underlying states, regulated by a matrix of transition probabilities $\mathbf{\Gamma}$. For
196 M states, $\mathbf{\Gamma}$ had dimensions $M \times M$ and each element $\gamma_{i,j}$ indicated the probability of being in state
197 j at time t, given that the animal was in state i at time $t - 1$. The Markov property was assumed
198 for the time series of states, i.e. state at time t only depended on state at time $t - 1$. The state
199 process was informed by the four variables, step length, turning angle, altitude and hierarchical
200 slope position, at time t. Given state $s_t = i$ (with i in 1,…,M), step lengths were modelled as
201 emerging from a Weibull distribution (McClintock et al., 2012; Morales et al., 2004), with state-
202 specific scale (α_i) and shape (β_i) parameters, determining the average step length per state and its
203 variability, i.e. $x_t \sim W(\beta_i, \alpha_i)$. Turning angles were assumed to have a wrapped Cauchy
204 distribution (McClintock et al., 2012; Morales et al., 2004) with mean (μ) equal to 0 and state-
205 specific concentration parameter (ρ_i), a measure of how angles are distributed around the mean,
206 i.e. $\theta_t \sim wC(0, \rho_i)$ (Breed, Costa, Jonsen, Robinson, & Mills-Flemming, 2012). The parameter ρ_i
207 varies between 1 (angles concentrated around the mean 0, i.e. directed movement) and 0
208 (corresponding to directions uniformly distributed on the circle, i.e. a classic random walk
209 allowing for convoluted movement). True, unobserved altitude at each minute t was modelled as
210 a random walk Gaussian variable with state-dependent standard deviation σ_i (Isojunno & Miller,
211 2015; Langrock, Marques, Baird, & Thomas, 2014), $\upsilon_t \sim N(\upsilon_{t-1} + \pi_i, \sigma_i)$, where υ_{t-1} is the true
212 altitude in the previous minute and π_i denotes the state-specific mean vertical drift, i.e. the
213 change in altitude between minutes. A Gaussian observation model accounted for errors in
214 altitude measurement, i.e. $a_t \sim N(\upsilon_t, \varepsilon)$. Finally, following data exploration, hierarchical slope
215 position was assumed to emerge from a Gaussian distribution with state-specific mean κ_i and
216 standard deviation ω_i, i.e. $h_t \sim N(\kappa_i, \omega_i)$.

We tested several alternative structures for the model, including a range of potential latent states (three to six). A model with five states converged successfully and aligned with biological expectations, so only this parameterisation is presented here. It is important to note that, in an unsupervised inference setting such as this (i.e. one where the true states are unknown), the number of states is driven by the process generating observed data (Leos-Barajas et al., 2017). However, the use of appropriate movement and ancillary environmental variables, capturing relevant features of an animal's behaviour, can lead to the identification of biologically meaningful latent states (Leos-Barajas et al., 2017; McClintock et al., 2013). The five states used here were characterised by features of the response variables that broadly corresponded to directed thermal soaring (state 1), gliding (state 2), convoluted thermal soaring (state 3), perching (or on the ground; state 4) and orographic soaring (but potentially including periods of flapping flight; state 5).

Priors

Following initial data exploration, a set of constraints was applied to the priors of state-specific parameters in order to facilitate model convergence and support the identification and assignment of functionally relevant latent states (Isojunno & Miller, 2015) (Appendix S1). This also prevented label switching, i.e. the non-identifiability of state-dependent components due to the posterior distribution being invariant to permutation of state labels (Stephens, 2000). These constraints were broad, and were only defining the overall tendency of the vertical movement (ascending, descending or stable overall) and the relative degree of directedness, speed and topographic exposure among states (Appendix S1). The standard deviation of the observation

model for altitude (ε) was set at a fixed value (25 m), but was large enough to conservatively account for the declared accuracy level (Lanzone et al., 2012).

Model fitting

The model was fitted using JAGS run from R (package runjags; Appendix S2) (Denwood, 2016). Markov chain Monte Carlo (MCMC) algorithms were iterated until convergence of the latent states and model parameters. State convergence was assessed by monitoring the proportion $\delta_{1,\ldots,5}$ of minutes classified under each latent state. We ran three parallel chains, starting at different initial values. Convergence was assessed by visually inspecting trace and density plots (Lunn, Jackson, Best, Thomas, & Spiegelhalter, 2013), and confirmed by checking that the Brooks-Gelman-Rubin (BGR) diagnostic fell below 1.1, and that Monte Carlo (MC) error was less than 5% of the sample standard deviation (Lunn et al., 2013). The R package coda was used to assess convergence, calculate effective sample size and extract posterior estimates (Plummer, Best, Cowles, & Vines, 2006).

Model validation

To investigate the model's ability to characterise functional latent states, we compared the model's posterior state classifications with existing manual behavioural classifications for a subset of tagged eagles. Particularly, data from 13 of the 48 spring tracks were previously evaluated manually as part of a prior study (Katzner et al., 2015). Flight modes were identified by an expert observer (T. A. Miller) based on the patterns of sequential GPS locations and on their overlap with topographical features. As a result, flight mode was classified into one of four states: thermal soaring, gliding, orographic soaring, and unknown (Katzner et al., 2015). Model state classifications were obtained from the posterior median estimate of the categorical state.

States 1 and 3 were combined and matched to manually-classified thermal soaring, state 2 was matched to manually-classified gliding, and state 5 to manually-classified orographic soaring. Manual and model classifications were compared using confusion matrices. Because the model could not assign an "unknown" state and accuracy could not be evaluated for "unknown" segments, accuracy estimates from this matrix will be artificially low. In addition, we tested whether the occurrence of gaps in the tracking data and measurement error in the horizontal and vertical dimension could affect the results, using a simulation procedure based on the posterior estimates of model parameters (Appendix S4) and carried out posterior predictive checks to assess the goodness-of-fit of the model to the data (Appendix S5).

Behavioural models

The results of the state-space model can be used to explore the ecology of the study species. To demonstrate this application, we carried out a descriptive investigation of the seasonal, age and sex differences in flight strategy and performance. Specifically, we fitted binomial mixed-effects models (package lme4 in R; Bates, Maechler & Bolker 2012) to test whether the proportional occurrence of each behavioural state (directed thermal soaring, convoluted thermal soaring, gliding and orographic soaring) in a track varied as a function of the interaction between season (autumn and spring) and age category (adults and sub-adults). Because this analysis aimed to compare the occurrence of flight modes, steps classified as on the ground or perching were excluded. Moreover, due to the small sample size, tracks of juveniles were also excluded. In a separate model, we tested for the effect of sex on the flight performance of adult eagles in the two seasons (we excluded sub-adults since most of them were males). Because individuals were tracked over multiple years, we included a random effect of individual and year in all models.

282 The random effects structure, as well as the inclusion of the fixed effects, was assessed using the
283 Akaike's information criterion (Gurka, 2006), corrected for small sample sizes (AICc).

284

285 **Results**

286 The 58 filtered eagle tracks corresponded to 72,844 GPS fixes, which made up 599 segments
287 longer than 10 min and separated from one another by more than 5 min. Regularisation of the
288 599 segments at a one-minute resolution reduced the sample analysed to 45,914 locations.

289 *State-space model*

290 Visual inspection of trace plots suggested that the chains were randomly oscillating around a
291 central value after 5,000 iterations, so these initial draws were discarded as burn-in. Diagnostics
292 confirmed that the model converged adequately after 15,000 iterations (Table S3). We also
293 verified that these iterations corresponded to an effective size of the posterior sample greater than
294 400 for all parameters (Lunn et al., 2013). Due to computing memory limitations, we only
295 retained one in 10 iterations.

296 The results were consistent with our biological expectations of eagle behaviour, embedded in the
297 priors, while describing the features of each state precisely. Under state 1 (directed thermal
298 soaring), an individual gained substantial altitude and moved in large, directed steps. State 3
299 (convoluted thermal soaring) was similar to state 1, but steps were considerably shorter and
300 turning angles had low concentration. Bouts of both states appeared to be followed by gliding
301 periods (state 2). State 4 (on the ground or perching) was characterised by extremely small and
302 convoluted horizontal steps, and visual investigation of the tracks confirmed it corresponded to

303 periods when an eagle was not moving (e.g. Fig. S2). Finally, state 5 (orographic soaring)
304 showed large variation in the vertical drift, suggesting irregular gaining and losing of altitude.
305 This flight mode was correctly classified to occur over topographies characterised by high
306 exposure (such as ridgelines). The posterior distributions of the state-dependent parameters are
307 summarised in Table S3 and the emission distributions of the four response variables (step
308 length, turning angle, vertical drift and hierarchical slope position) are plotted in Fig. S1.

309 The posterior median was used to classify the behavioural state at each time step. The
310 comparison of model state classifications with manually classified flight modes returned a mean
311 of 68% correct classifications across states (Table S4; 67% for thermal soaring, 70% for gliding
312 and 65% for orographic soaring). As an example, we plotted four track segments coloured by
313 state, where posterior true altitude values were used (Fig. 2). Based on posterior state
314 classifications, we calculated eagles' activity budget, across both migration seasons and by
315 migration season (Table 1). These data suggested that orographic soaring was less frequent in
316 spring than in autumn.

317 The model also appeared to be robust to observed levels of sampling irregularity and
318 measurement errors (Appendix S4). However, the posterior predictive checks highlighted
319 potential issues with the validity of the Markov property given the small time interval between
320 observations (Appendix S5, Figs. S4 and S5).

321 *Behavioural models*

322 Model selection highlighted differences among individuals and among years in the occurrence of
323 most flight modes (Table S5; Fig. S3). The use of orographic soaring varied by age category and
324 season, suggesting that this flight mode occurred proportionally more in autumn and was used

more by sub-adults (Fig. 3a). In contrast, directed thermal soaring occurred more in spring and was used more by adults (Fig. 3a). Convoluted thermal soaring appeared to be used more by sub-adults in autumn and by adults in spring, but the estimated effects had wide confidence intervals (Fig. 3a). Gliding occurred more in spring, and was used more by adults, although the latter effect showed large confidence intervals (Fig. 3a). Model results also suggested that the proportional occurrence of orographic soaring and gliding varied between the sexes, but differently in the two seasons. Females used more orographic soaring and less gliding than males, but only in autumn (Fig. 3b). No difference between the sexes was found for directed or convoluted thermal soaring (Table S5).

Discussion

To our knowledge, this study represents the first example of the use of altitude measurements in conjunction with horizontal information and ancillary environmental variables in hidden state models to characterise functional behavioural modes in three dimensions (McClintock, London, Cameron, & Boveng, 2017; McClintock et al., 2013). This is particularly useful for flying organisms, where studying the variation in flight mode might be more relevant than simply distinguishing resident and transit movement identified by models in two dimensions (Jonsen et al., 2013). In addition to identifying expected behavioural states of golden eagles, our model was able to tease apart two types of thermal soaring with different directedness. Previous work has generally classified thermal soaring as a single category of behaviour (e.g. Katzner et al., 2015), while the combination of horizontal and vertical information in our study discriminated additional flight features. The degree of directedness while gaining altitude within a thermal is

likely dependent upon the strength and distribution of thermals, the alignment of thermals with flight direction, and wind conditions (Kerlinger, 1989). Whenever conditions cause thermals to drift, birds using this form of soaring will also drift, resulting in straighter movement (Hedenström & Alerstam, 1995). This can warrant faster forward progress with the same energy expenditure, but only if the thermals drift in the same direction as the primary axis of movement. However, most thermal soaring was convoluted, because stronger winds disrupt thermal lift (Kerlinger, 1989). Where the data exist, our approach could be used to test this hypothesis by including an explicit effect of wind speed.

The identification of behavioural states makes it possible to describe time allocation to different movement modes. This can shed light on an animal's decision-making process as it moves through space and adjusts to environmental conditions (Nathan et al., 2008) with flight modes of different efficiencies (Duerr et al., 2012). For example, eagles used different strategies to migrate depending on the season, as reflected in the higher occurrence of orographic flight in autumn and the higher occurrence of gliding and directed thermal soaring in spring. This is intuitive, since the availability of thermals is higher in spring (Duerr et al., 2015).

The behavioural models also highlighted differences in flight strategy and performance between age categories. Across both seasons, adults used gliding and directed thermal soaring more than sub-adults, which in turn used more orographic soaring, although these patterns were not reflected in the results for convoluted thermal soaring. Previous studies suggested that, in spring, adults need to move quickly towards the reproductive areas to secure nesting territories, while sub-adults can delay their migration and wait for energetically optimal weather conditions (Duerr et al., 2015; Miller et al., 2016). During spring migration, the relative use of different flight

369 modes also changes as a result of these processes (Katzner et al., 2015). In contrast, our results
370 highlight that, at a broader scale, adults' experience allows them to rely on more efficient flight
371 modes compared to sub-adults overall, despite the constraints of reproduction. This
372 inconsistency with previous work may also be a by-product of the disproportionate classification
373 of behavioural states manually identified as 'unknown' into thermal soaring (Table S4).

374 We also found substantial individual and yearly variability in flight performance, as well as
375 differences in the use of orographic soaring and directed thermal soaring between males and
376 females in autumn (Table S5). The larger size of females and corresponding higher weight might
377 explain some of these patterns, although further investigation is required to explore the
378 underlying functional processes. Because flight modes are characterised by different energetic
379 investment and movement efficiency (Duerr et al., 2012; Hedenstrom, 1993; Hedenström &
380 Alerstam, 1995), their variation among years, seasons, ages, sexes and individuals is relevant for
381 an individual's energy budget, which will ultimately affect its ability to survive and reproduce
382 successfully (Weimerskirch, Louzao, de Grissac, & Delord, 2012). Investigating any spatial or
383 temporal patterns in flight mode distribution could therefore highlight the moments in time or
384 areas that are critical in terms of energy requirements during migration (Shepard et al., 2013).
385 The energetic insight our model can provide also suggests its relevance to the study of other
386 organisms' flight modes and their variation in space and time (Alexander, 2015).

387 Beyond energetics, characterising behavioural states in flying animals is particularly important to
388 evaluate their susceptibility to human activities, informing effective planning and management
389 (Katzner, Brandes, et al., 2012; Péron et al., 2017; Ross-Smith et al., 2016). For example,
390 specific behavioural states, due to their horizontal and vertical characteristics, may put birds at

391 higher risk of collision with turbines (Ross-Smith et al., 2016). For golden eagles in eastern
392 North America, the spatiotemporal distribution of flight modes could be mapped to quantify their
393 overlap with wind power developments within the population's range (Miller et al., 2014) and
394 inform simulation models that estimate collision rates (New, Bjerre, Millsap, Otto, & Runge,
395 2015). In this sense, the mismatch between manual and model classifications may be irrelevant
396 as long as movement features are described correctly, because vulnerability in a state may be
397 more related to average altitude and speed, rather than the type of updraft birds are using.

398 Given that migration patterns are highly affected by weather conditions (Duerr et al., 2015;
399 Lanzone et al., 2012; Miller et al., 2016), the viability of this, and other, populations of long-
400 ranging migratory birds is also threatened by global climate changes (Møller, Rubolini, &
401 Lehikoinen, 2008). The presence of two types of thermal soaring suggests sensitive responses by
402 birds to variation in weather. Thus, major alterations of wind patterns and the increase in
403 frequency of extreme weather events may affect flight decisions and energetic efficiency,
404 potentially compromising birds' migratory abilities (Marra, Francis, Mulvihill, & Moore, 2005).
405 Our model could be used to assess changes in activity budgets following altered weather
406 conditions. In turn, a modified allocation of time to activities with different energetic efficiency
407 could affect the energy balance of these species over the migration and, ultimately, have
408 consequences on their survival and reproductive success (Weimerskirch et al., 2012).

409 From a methodological perspective, the state-space framework presented here advances previous
410 work that modelled altitude data in isolation (Ross-Smith et al., 2016). In addition to altitude, it
411 was the use of ancillary topographical information that supported the identification of orographic
412 soaring, which is associated with ridges and other structures deflecting horizontal winds

413 (Kerlinger, 1989; Mallon, Bildstein, & Katzner, 2016). Selecting appropriate ancillary metrics is
414 critical for the successful discrimination of flight modes that are promoted by specific features of
415 the environment (Murphy et al., 2010). Our analytical approach was unsupervised, in the sense
416 that observed behavioural states were not used to tune the model (Leos-Barajas et al., 2017).
417 However, as part of the preliminary exploration of the tracking dataset, five states were selected
418 and suitable constraints were set to broadly match these states with potential flight modes. The
419 fitting procedure returned posterior estimates of state-specific parameters that were consistent
420 with initial observations and described these putative states in detail.

421 The approach we used aligns with recent analytical efforts to characterise diving and underwater
422 foraging behaviour by marine mammals and seabirds, where depth is used as the third dimension
423 instead of altitude (Bestley et al., 2015; Dean et al., 2013; Isojunno & Miller, 2015; Langrock et
424 al., 2014; Quick et al., 2017). Together with these studies from the marine realm, it therefore
425 represents a step towards developing a fully three-dimensional movement model as data from
426 new sensors (e.g. accelerometry) become available (Leos-Barajas et al., 2017). To this purpose, a
427 semi-Markov extension of the model might be considered (Isojunno & Miller, 2015; Langrock et
428 al., 2014). The distribution of the durations of stays in the various flight modes is unlikely to be
429 geometric, as implied by the Markov property (Langrock et al., 2014), particularly when using a
430 short time step. The posterior predictive checks on our model confirmed that there was residual
431 autocorrelation for some of the response variables under some states (Appendix S5). While this
432 assumption may not affect appropriate behavioural classification, it becomes important when
433 estimated probabilities are used to simulate new tracks.

434

Conclusions

The proliferation of bio-logging devices offers the unique opportunity of detailing individuals' behavioural patterns at nested scales (Nathan et al., 2008). Identifying different behavioural modes that arise from animals' response to the underlying habitat and quantifying their spatiotemporal variation can provide valuable insights into the mechanisms driving behavioural, energetic and, in the long term, life history decisions (Hays et al., 2016). However, new statistical tools are required to explore these large datasets and summarise the wide range of movement features into understandable states (Patterson et al., 2008). Here, we presented a model that describes a bird's latent behaviour as it switches among flight modes during migration. Model results highlighted two different patterns of thermal soaring flight. Moreover, the analysis of the relative occurrence of different flight modes showed yearly, seasonal, individual, age and sex differences in flight strategy and performance, shedding light on the functional processes underlying individual behavioural patterns in the context of a dynamic environment.

Acknowledgements

Funding for telemetry of eagles and database maintenance and analysis was received from the Virginia Department of Game and Inland Fisheries through a Federal Aid in Wildlife Restoration grant from USFWS, Pennsylvania SWG grants T-12 and T47-R-1, US DoE grant DEEE0003538, Charles A. and Anne Morrow Lindbergh Foundation, and the authors' organizations. Jeff Cooper, Michael Lanzone, Kieran O'Malley and many others assisted with numerous phases of this research. Adam Kane, Theoni Photopoulou, Saana Isojunno contributed

457 useful discussions on hidden state models. Michael Runge provided valuable comments on an
458 earlier version of this manuscript. Emer Rogan and University College Cork provided desk space
459 to EP. Any use of trade, product, or firm names is for descriptive purposes only and does not
460 imply endorsement by the U.S. Government.

461

462 **Authors' contributions:** All authors contributed to discussions that led to the development of
463 the research project; TM, MB, TK and AD collected and managed eagle telemetry data; EP and
464 LN developed the modelling approach, EP led that exercise and the writing and all authors
465 contributed to revisions.

466

467 **Data accessibility**

468 Data will be made publicly available upon acceptance.

469

470 **References**

471 Alexander, D. E. (2015). *On the wing: insects, pterosaurs, birds, bats and the evolution of*
472 *animal flight*. Oxford University Press, Oxford, UK.

473 Barrios, L., & Rodríguez, A. (2004). Behavioural and environmental correlates of soaring-bird
474 mortality an an-shore wind turbines. *Journal of Applied Ecology*, *41*(1), 72–81.
475 doi:10.1111/j.1365-2664.2004.00876.x

476 Bates, D., Maechler, M., & Bolker, B. (2012). lme4: Linear mixed-effects models using S4

classes. R package version 0.999999-0. Available at: http://cran.r-project.org/package=lme4.

Bestley, S., Jonsen, I., Hindell, M., Harcourt, R. G., & Gales, N. (2015). Taking animal tracking to new depths: synthesizing horizontal–vertical movement relationships for four marine predators. *Ecology*, *96*(2), 417–427. doi:10.1890/14-0469.1

Breed, G. a., Costa, D. P., Jonsen, I. D., Robinson, P. W., & Mills-Flemming, J. (2012). State-space methods for more completely capturing behavioral dynamics from animal tracks. *Ecological Modelling*, *235–236*, 49–58. doi:10.1016/j.ecolmodel.2012.03.021

Dean, B., Freeman, R., Kirk, H., Leonard, K., Phillips, R. A., Perrins, C. M., & Guilford, T. (2013). Behavioural mapping of a pelagic seabird: combining multiple sensors and a hidden Markov model reveals the distribution of at-sea behaviour. *Journal of the Royal Society Interface*, *10*(78), 20120570. doi:10.1098/rsif.2012.0570

Dennhardt, A. J., Duerr, A. E., Brandes, D., & Katzner, T. E. (2015). Integrating citizen-science data with movement models to estimate the size of a migratory golden eagle population. *Biological Conservation*, *184*, 68–78. doi:10.1016/j.biocon.2015.01.003

Denwood, M. J. (2016). runjags: An R package providing interface utilities, model templates, parallel computing methods and additional distributions for MCMC models in JAGS. *Journal of Statistical Software*, *71*(9), 1–25.

Duerr, A. E., Miller, T. A., Lanzone, M., Brandes, D., Cooper, J., O'Malley, K., … Katzner, T. (2012). Testing an emerging paradigm in migration ecology shows surprising differences in efficiency between flight modes. *PLoS ONE*, *7*(4), e35548.

498 doi:10.1371/journal.pone.0035548

499 Duerr, A. E., Miller, T. A., Lanzone, M., Brandes, D., Cooper, J., O'Malley, K., … Katzner, T.
500 (2015). Flight response of slope-soaring birds to seasonal variation in thermal generation.
501 *Functional Ecology*, *29*(6), 779–790. doi:10.1111/1365-2435.12381

502 Evans, J. (2017). spatialEco. R package version 0.0.1-7. <URL: https://CRAN.R-
503 project.org/package=spatialEco>.

504 Gurka, M. J. (2006). Selecting the best linear mixed model under REML. *American Statistician*,
505 *60*(1), 19–26. doi:10.1198/000313006X90396

506 Hays, G. C., Ferreira, L. C., Sequeira, A. M. M., Meekan, M. G., Duarte, C. M., Bailey, H., …
507 Thums, M. (2016). Key questions in marine megafauna movement ecology. *Trends in*
508 *Ecology and Evolution*, *31*(6), 463–475. doi:10.1016/j.tree.2016.02.015

509 Hedenstrom, A. (1993). Migration by soaring or flapping flight in birds: The relative importance
510 of energy cost and speed. *Philosophical Transactions of the Royal Society B: Biological*
511 *Sciences*, *342*(1302), 353–361. doi:10.1098/rstb.1993.0164

512 Hedenström, A., & Alerstam, T. (1995). Optimal flight speed of birds. *Philosophical*
513 *Transactions of the Royal Society B: Biological Sciences*, *348*(1326), 471–487.
514 doi:10.1098/rstb.1995.0082

515 Isojunno, S., & Miller, P. J. O. (2015). Sperm whale response to tag boat presence: biologically
516 informed hidden state models quantify lost feeding opportunities. *Ecosphere*, *6*(1), 1–46.
517 doi:10.1890/ES14-00130.1

518 Jonsen, I., Basson, M., Bestley, S., Bravington, M. V., Patterson, T. A., Pedersen, M. W., …

519 Wotherspoon, S. J. (2013). State-space models for bio-loggers: A methodological road map.
520 *Deep Sea Research Part II: Topical Studies in Oceanography*, *88–89*, 34–46.
521 doi:10.1016/j.dsr2.2012.07.008

522 Katzner, T. E., Brandes, D., Miller, T., Lanzone, M., Maisonneuve, C., Tremblay, J. A., …
523 Merovich, G. T. (2012). Topography drives migratory flight altitude of golden eagles:
524 Implications for on-shore wind energy development. *Journal of Applied Ecology*, *49*(5),
525 1178–1186. doi:10.1111/j.1365-2664.2012.02185.x

526 Katzner, T. E., Smith, B. W., Miller, T. A., Brandes, D., Cooper, J., Brauning, D., … Bildstein,
527 K. L. (2012). Status, biology, and conservation priorities for North America's eastern
528 Golden Eagle (*Aquila chrysaetos*) population. *The Auk*, *129*, 168–176.

529 Katzner, T. E., Turk, P. J., Duerr, A. E., Miller, T. A., Lanzone, M. J., Cooper, J. L., …
530 Lemaître, J. (2015). Use of multiple modes of flight subsidy by a soaring terrestrial bird, the
531 golden eagle *Aquila chrysaetos*, when on migration. *Journal of the Royal Society Interface*,
532 *12*, 20150530. doi:10.1098/rsif.2015.0530

533 Kays, R., Crofoot, M. C., Jetz, W., & Wikelski, M. (2015). Terrestrial animal tracking as an eye
534 on life and planet. *Science*, *348*(6240), 1222–1232. doi:10.1126/science.aaa2478

535 Kerlinger, P. (1989). *Flight strategies of migrating hawks*. University of Chicago Press, Chicago.

536 Klaassen, R. H. G., Strandberg, R., Hake, M., & Alerstam, T. (2008). Flexibility in daily travel
537 routines causes regional variation in bird migration speed. *Behavioral Ecology and*
538 *Sociobiology*, *62*(9), 1427–1432. doi:10.1007/s00265-008-0572-x

539 Langrock, R., King, R., Matthiopoulos, J., Thomas, L., Fortin, D., & Morales, J. M. (2012).

Flexible and practical modeling of animal telemetry data: hidden Markov models and extensions. *Ecology*, *93*(11), 2336–2342. doi:10.1371/journal.pbio.1000178

Langrock, R., Marques, T. A., Baird, R. W., & Thomas, L. (2014). Modeling the diving behavior of whales: A latent-variable approach with feedback and semi-Markovian components. *Journal of Agricultural, Biological, and Environmental Statistics*, *19*(1), 82–100. doi:10.1007/s13253-013-0158-6

Lanzone, M. J., Miller, T. A., Turk, P., Brandes, D., Halverson, C., Maisonneuve, C., … Katzner, T. (2012). Flight responses by a migratory soaring raptor to changing meteorological conditions. *Biology Letters*, *8*(5), 710–713. doi:10.1098/rsbl.2012.0359

Leos-Barajas, V., Photopoulou, T., Langrock, R., Patterson, T. A., Watanabe, Y. Y., Murgatroyd, M., & Papastamatiou, Y. P. (2017). Analysis of animal accelerometer data using hidden Markov models. *Methods in Ecology and Evolution*, *8*, 161–173. doi:10.1111/2041-210X.12657

Lunn, D., Jackson, C., Best, N., Thomas, A., & Spiegelhalter, D. (2013). *The BUGS book: A practical introduction to Bayesian analysis*. Boca Raton, Florida, USA: Chapman & Hall/CRC.

Mallon, J. M., Bildstein, K. L., & Katzner, T. E. (2016). In-flight turbulence benefits soaring birds. *Auk*, *133*(1), 79–85. doi:10.1642/AUK-15-114.1

Marra, P. P., Francis, C. M., Mulvihill, R. S., & Moore, F. R. (2005). The influence of climate on the timing and rate of spring bird migration. *Oecologia*, *142*(2), 307–315. doi:10.1007/s00442-004-1725-x

McClintock, B. T., King, R., Thomas, L., Matthiopoulos, J., McConnell, B. J., & Morales, J. M. (2012). A general discrete-time modeling framework for animal movement using multistate random walks. *Ecological Monographs*, *82*(3), 335–349. doi:10.1890/11-0326.1

McClintock, B. T., London, J. M., Cameron, M. F., & Boveng, P. L. (2017). Bridging the gaps in animal movement: Hidden behaviors and ecological relationships revealed by integrated data streams. *Ecosphere*, *8*(3). doi:10.1002/ecs2.1751

McClintock, B. T., Russell, D. J. F., Matthiopoulos, J., & King, R. (2013). Combining individual animal movement and ancillary biotelemetry data to investigate population-level activity budgets. *Ecology*, *94*(4), 838–849.

Michelot, T., Langrock, R., Bestley, S., Jonsen, I. D., Photopoulou, T., & Patterson, T. A. (2017). Estimation and simulation of foraging trips in land-based marine predators. *Ecology*, *98*(7), 1932–1944. doi:10.1002/ecy.1880

Miller, T. A., Brooks, R. P., Lanzone, M., Brandes, D., Cooper, J., O'Malley, K., … Katzner, T. (2014). Assessing risk to birds from industrial wind energy development via paired resource selection models. *Conservation Biology*, *28*(3), 745–755. doi:10.1111/cobi.12227

Miller, T. A., Brooks, R. P., Lanzone, M. J., Brandes, D., Cooper, J., Tremblay, J. A., … Katzner, T. E. (2016). Limitations and mechanisms influencing the migratory performance of soaring birds. *Ibis*, *158*, 116–134. doi:10.1111/ibi.12331

Møller, A. P., Rubolini, D., & Lehikoinen, E. (2008). Populations of migratory bird species that did not show a phenological response to climate change are declining. *Proceedings of the National Academy of Sciences of the United States of America*, *105*(42), 16195–16200.

doi:10.1073/pnas.0803825105

Morales, J. M., Haydon, D. T., Frair, J., Holsinger, K. E., & Fryxell, J. M. (2004). Extracting more out of relocation data: building movement models as mixtures of random walks. *Ecology*, *85*(9), 2436–2445. doi:10.1890/03-0269

Murphy, M. A., Evans, J. S., & Storfer, A. (2010). Quantifying Bufo boreas connectivity in Yellowstone National Park with landscape genetics. *Ecology*, *91*(1), 252–61. doi:10.1890/08-0879.1

Nathan, R., Getz, W. M., Revilla, E., Holyoak, M., Kadmon, R., Saltz, D., & Smouse, P. E. (2008). A movement ecology paradigm for unifying organismal movement research. *Proceedings of the National Academy of Sciences*, *105*(49), 19052–19059. doi:10.1073/pnas.0800375105

New, L., Bjerre, E., Millsap, B., Otto, M. C., & Runge, M. C. (2015). A collision risk model to predict avian fatalities at wind facilities: An example using golden eagles, *Aquila chrysaetos*. *PLoS ONE*, *10*(7), 1–12. doi:10.1371/journal.pone.0130978

Patterson, T. A., Thomas, L., Wilcox, C., Ovaskainen, O., & Matthiopoulos, J. (2008). State-space models of individual animal movement. *Trends in Ecology & Evolution*, *23*(2), 87–94. doi:10.1016/j.tree.2007.10.009

Péron, G., Fleming, C. H., Duriez, O., Fluhr, J., Itty, C., Lambertucci, S., … Calabrese, J. M. (2017). The energy landscape predicts flight height and wind turbine collision hazard in three species of large soaring raptor. *Journal of Applied Ecology*, *54*(6), 1895–1906. doi:10.1111/1365-2664.12909

Pirotta, E., Edwards, E. W. J., New, L., & Thompson, P. M. (2018). Central place foragers and moving stimuli: a hidden-state model to discriminate the processes affecting movement. *Journal of Animal Ecology*, *In press*. doi:10.1111/1365-2656.12830

Plummer, M., Best, N., Cowles, K., & Vines, K. (2006). CODA: Convergence Diagnosis and Output Analysis for MCMC. *R News*, *6*, 7–11.

Poessel, S. A., Duerr, A. E., Hall, J. C., Braham, M. A., & Katzner, T. E. (2018). Improving estimation of flight altitude in wildlife telemetry studies. *Journal of Applied Ecology*, 1–7. doi:10.1111/1365-2664.13135

Quick, N. J., Isojunno, S., Sadykova, D., Bowers, M., Nowacek, D. P., & Read, A. J. (2017). Hidden Markov models reveal complexity in the diving behaviour of short-finned pilot whales. *Scientific Reports*, *7*, 45765. doi:10.1038/srep45765

R Development Core Team. (2016). R: A language and environment for statistical computing. R Foundation for Statistical Computing, Vienna, Austria. ISBN 3-900051-07-0, URL http://www.R-project.org/.

Ross-Smith, V. H., Thaxter, C. B., Masden, E. A., Shamoun-Baranes, J., Burton, N. H. K., Wright, L. J., … Thompson, D. (2016). Modelling flight heights of lesser black-backed gulls and great skuas from GPS: a Bayesian approach. *Journal of Applied Ecology*, *53*(6), 1676–1685. doi:10.1111/1365-2664.12760

Shepard, E. L. C., Wilson, R. P., Rees, W. G., Grundy, E., Lambertucci, S. A., & Vosper, S. B. (2013). Energy landscapes shape animal movement ecology. *The American Naturalist*, *182*(3), 298–312. doi:10.1086/671257

624 Stephens, M. (2000). Dealing with label switching in mixture models. *Journal of the Royal*
625 *Statistical Society: Series B (Statistical Methodology)*, *62*(4), 795–809.

626 Weimerskirch, H., Louzao, M., de Grissac, S., & Delord, K. (2012). Changes in wind pattern
627 alter albatross distribution and life-history traits. *Science*, *335*, 211–214.
628 doi:10.1126/science.1210270

629 Williams, H. J., Shepard, E. L. C., Duriez, O., & Lambertucci, S. A. (2015). Can accelerometry
630 be used to distinguish between flight types in soaring birds? *Animal Biotelemetry*, *3*(1), 45.
631 doi:10.1186/s40317-015-0077-0

632

633 **Supporting Information**

634 Additional supporting information may be found in the online version of this article.

635 **Table S1.** Number of tracks available per individual in each year.

636 **Table S2.** Description of variables and model parameters.

637 **Appendix S1.** Details of prior distributions.

638 **Appendix S2.** JAGS code for the model.

639 **Table S3.** Posterior estimates of model parameters.

640 **Figure S1.** State-dependent emission distributions of the four response variables.

641 **Figure S2.** Example of time series of true altitudes from a track segment.

642 **Table S4.** Confusion matrix comparing manual and model state classifications.

643 **Table S5.** Results of model selection for the behavioural models.

644 **Figure S3.** Dot plots of the random effects of individual and year.

645 **Appendix S3.** Reformulation of the model allowing for missing data.

646 **Appendix S4.** Analysis of simulated data.

647 **Appendix S5.** Posterior predictive checks.

648 **Figure S4**. Results of the posterior predictive checks.

649 **Figure S5.** Autocorrelation function (ACF) plots for the response variables by state in the
650 original and simulated data.

651 **Tables**

652

653 Table 1. Estimated golden eagle activity budget, across both migration seasons and by migration

654 season.

	Directed thermal soaring	*Gliding*	*Convoluted thermal soaring*	*On the ground or perching*	*Orographic soaring*
Overall	2%	31%	38%	9%	20%
Spring	3%	32%	37%	10%	18%
Autumn	0%	24%	43%	8%	25%

655

Figures

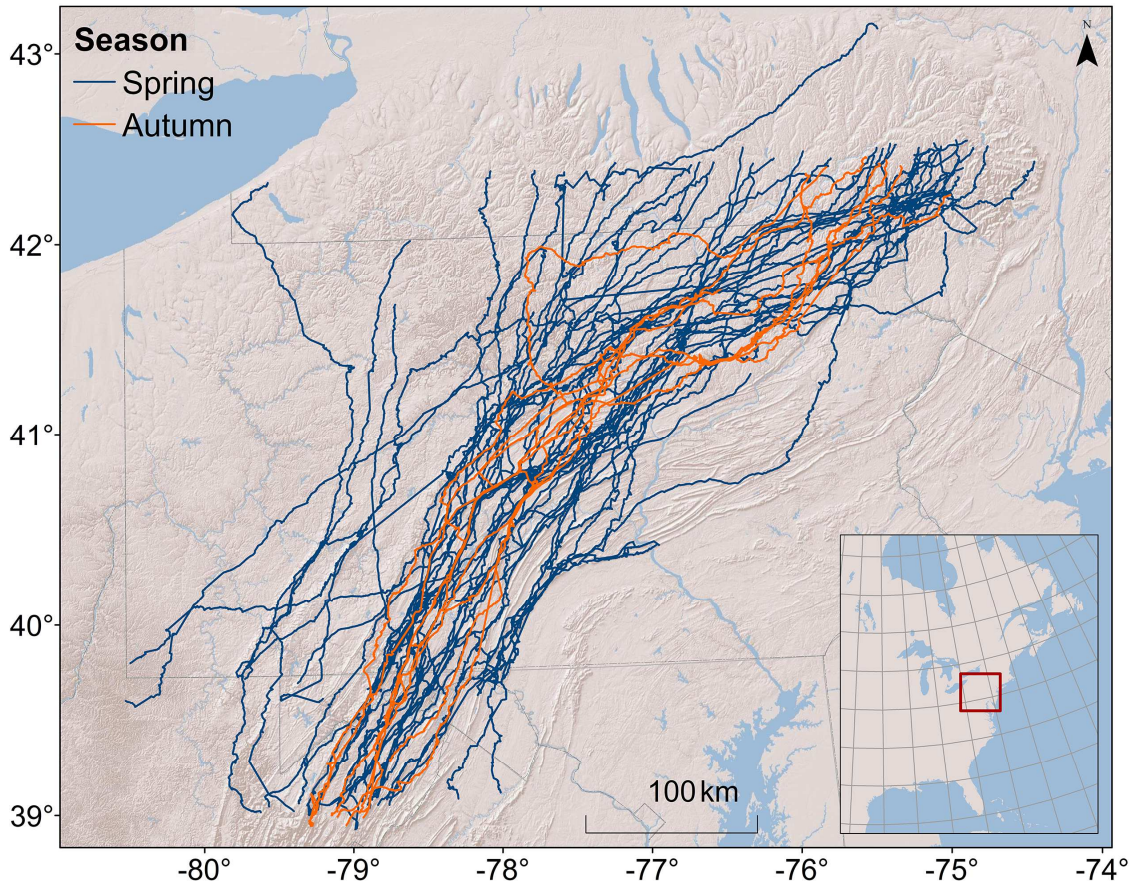
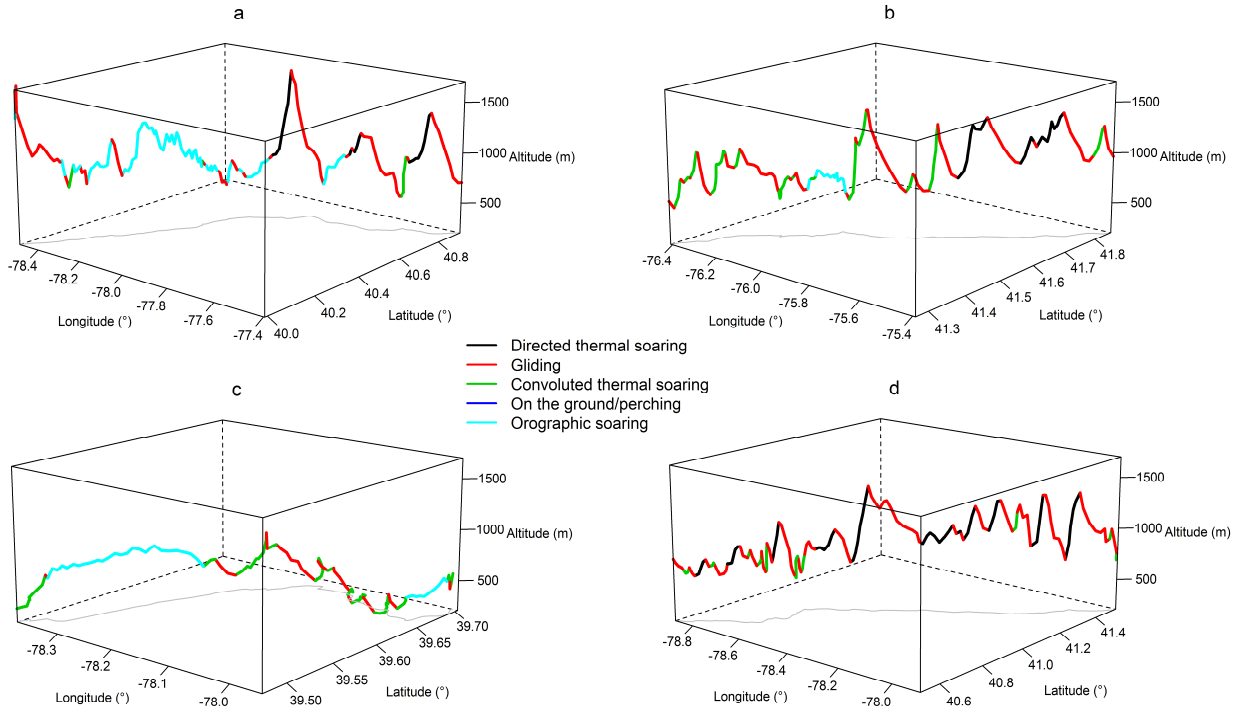


Figure 1. Map of study area and golden eagle tracks in autumn (48 tracks) and in spring (10 tracks).



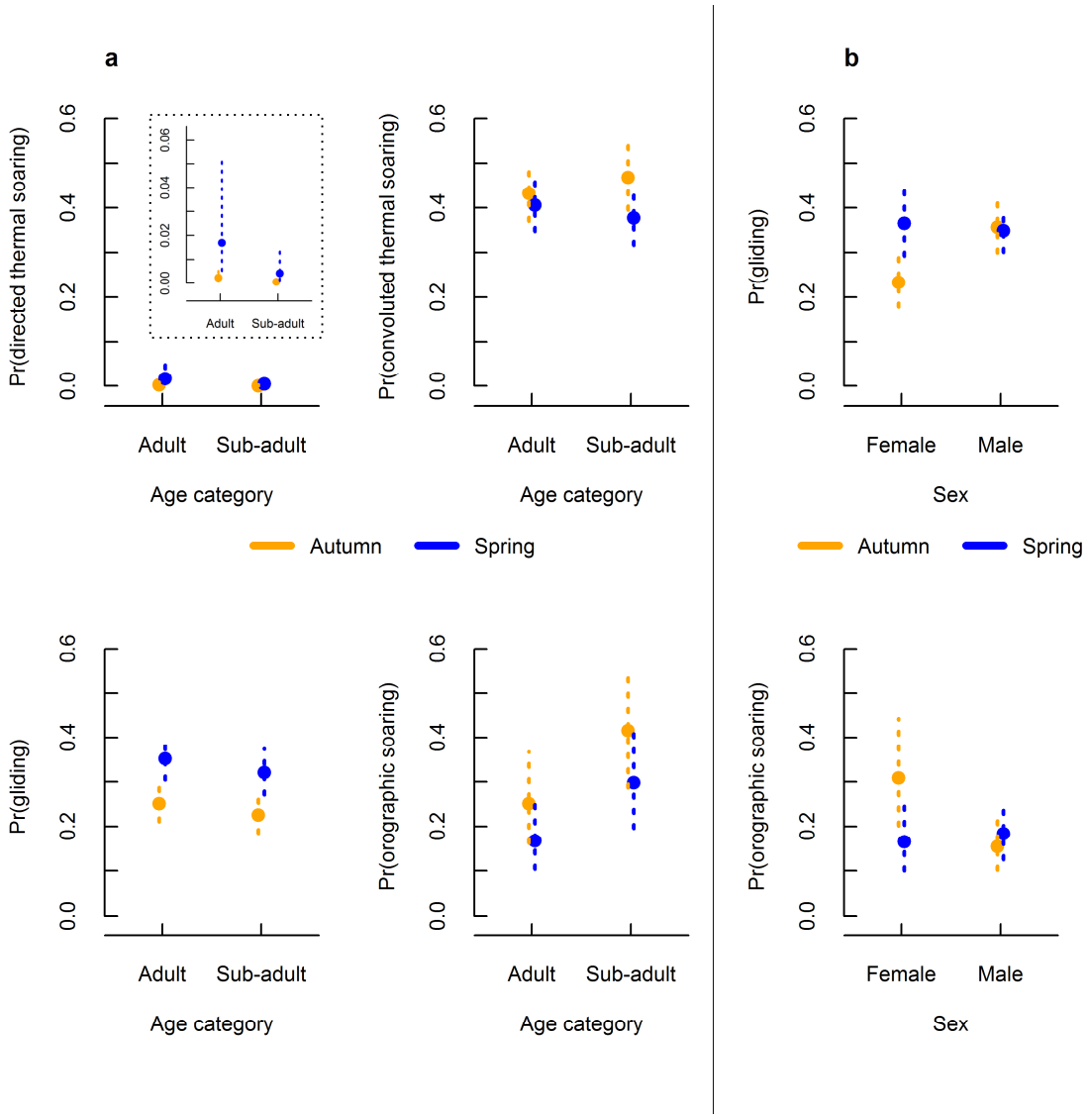
661

662 Figure 2. Segments of three-dimensional golden eagle tracks. Tracks are coloured based on

663 model posterior medians of the behavioural state at each minute *t*. In grey, the shadow of the

664 track projected onto the horizontal plane. The posterior median of true altitudes is used for the

665 vertical dimension.



666

667 Figure 3. Results of the behavioural models by state (mean and 95% confidence intervals). The
668 y-axis was standardised across plots, but the top left plot also includes a zoomed inset graph
669 (dotted box) for clarity. a) Effect of season and age category on the proportional occurrence of
670 each state. b) Effect of season and sex on the proportional occurrence of gliding and orographic
671 soaring. Results for the two forms of thermal soaring are not reported because the effect of sex
672 was not retained by model selection.

Supporting information

Table S1. Number of tracks available per individual in each year.

Individual ID	**Year**							
	2009	*2010*	*2011*	*2012*	*2013*	*2014*	*2015*	*2016*
95	0	0	2	1	0	0	0	0
301	0	1	0	0	0	0	0	0
376	0	1	0	0	0	0	0	0
434	0	0	1	0	0	0	0	0
483	0	0	1	0	0	0	0	0
558	0	0	1	0	0	0	0	0
749	0	0	1	0	0	0	0	0
2851	0	1	0	0	0	0	0	0
3206	0	0	1	0	0	0	0	0
3546	0	0	1	0	0	0	0	0
3553	0	1	0	0	0	0	0	0
3785	0	0	0	2	2	2	0	0
4189	0	0	0	1	0	0	0	0
4195	0	0	0	1	1	0	0	0
4379	0	0	0	2	1	2	1	1
4533	1	0	0	0	0	0	0	0
4733	0	1	1	1	1	1	1	0
4782	0	1	1	0	0	0	0	0
5061	0	0	0	0	1	0	0	0
5244	0	0	0	1	1	0	0	0
5269	0	0	0	2	2	1	0	0
6960	1	0	0	0	0	0	0	0
7231	0	0	0	2	1	1	0	0
7454	0	0	0	1	0	0	0	0
7878	0	0	2	1	0	0	0	0
8107	1	0	0	0	0	0	0	0
9013	0	0	0	1	0	0	0	0
9287	0	0	0	0	0	1	0	0

Table S2. Description of variables and model parameters. The subscript *t* indicates a time-dependent variable, while the subscript *i* indicates a state-dependent parameter. HSP stands for hierarchical slope position.

Class	Symbol	Name	Definition
Data	x_t	Step length	Distance between consecutive locations
	θ_t	Turning angle	Angle between consecutive steps
	a_t	Altitude (observed)	Altitude above sea level as measured by the GPS
	h_t	Hierarchical slope position	Measure of topographic exposure (Murphy, Evans, & Storfer, 2010)
	$\mathbf{y}_t$	Data vector	Vector of observations of the three movement metrics (x, θ, a and h)
Underlying variables	s_t	State	Latent behavioural state
	υ_t	Altitude (true)	True altitude above sea level
Model parameters	π_i	Vertical drift	Mean change in altitude under state i
	σ_i	Altitude standard deviation	State-specific variation around altitude change
	ε	Altitude observation error	Altitude uncertainty due to GPS measurement error
	ρ_i	Concentration	State-dependent variability in turning angles
	α_i	Scale	Scale parameter for the state-dependent distribution of step lengths
	β_i	Shape	Shape parameter for the state-dependent distribution of step lengths
	κ_i	Mean HSP	State-dependent mean of hierarchical slope position
	ω_i	Standard deviation HSP	State-dependent standard deviation of hierarchical slope position
	$\gamma_{i,j}$	Transition probability	Probability of switching between state i and state j
	φ_i	Initial state probability	Probability of being in state i at the start of a track

Appendix S1. Details of prior distributions.

Priors for state 1 (directed thermal soaring): The vertical drift had a truncated positive prior, so that under this state the bird was assumed to be gaining altitude. The variability in vertical drift was constrained between 0 and 150 m. Turning angles were assumed to be relatively more directed (i.e. concentration > 0.5) than in other states. Priors for parameters α and β were defined on a logarithmic scale to avoid meaningless negative values. The mean and standard deviation of hierarchical slope position was unconstrained.

Priors for state 2 (gliding): The vertical drift had the same absolute value and variability as in state 1, but opposite sign, i.e. the bird was decreasing its altitude. The distribution of turning angles was assumed to be the same as in state 1. This state had the same step length distribution as state 1. The mean and standard deviation of hierarchical slope position was the same as in state 1. We also investigated a model where the descending state (state 2) had the same horizontal features of state 3, but this model did not converge, suggesting that, while ascending behaviour can be either horizontally straight or convoluted, descending behaviour tends to be predominantly straight, as expected from gliding flight (Katzner et al., 2015).

Priors for state 3 (convoluted thermal soaring): The prior for vertical drift was truncated to represent altitude gain. The variability in vertical drift was constrained between 0 and 150 m. This state was constrained to be at most as directed as states 1, 2 and 5. Steps were constrained to be smaller than under state 1 and 2. The mean and standard deviation of hierarchical slope position was the same as in state 1 and 2.

Priors for state 4 (on the ground or perching): The bird was assumed to remain at a stable altitude, on average (i.e. mean vertical drift was set to 0, with a standard deviation fixed at 10 m

to represent small changes in altitude due to terrain features). Horizontal movement was assumed to be relatively more convoluted (i.e. concentration < 0.5). Steps were constrained to be smaller than under state 3.

Priors for state 5 (orographic soaring): The bird was assumed to remain at a stable altitude, on average (i.e. mean vertical drift was set to 0). The variability in vertical drift was constrained between 0 and 150 m. The distribution of turning angles was assumed to be the same as in state 1. Steps were constrained to be smaller than under state 1 and 2. Hierarchical slope position has higher values along ridges and was thus assumed to have mean higher in this state than in state 1, 2 and 3, while its variability was unconstrained.

States at time *t* were not previously labelled, and the model assigned a state to each time step based on the posterior estimates of the parameters. We used an unbiased and relatively uninformative Dirichlet(1,1,1,1,1) prior for the transition probabilities $\gamma_{i,1\ldots5}$ from each state *i* to all states, as well as for the probabilities of being in each state at the beginning of a track or track segment $\varphi_{1,\ldots,5}$. The standard deviation of the observation model for altitude (ε) was set to 25 m. While it would be preferable to estimate this parameter directly from the data, such standard deviation was found to be confounded with the standard deviation of true altitude. However, the fixed value we used was larger than the reported accuracy of the GPS devices (± 15 m; Lanzone et al., 2012), as a conservative way to account for error variation due to fix quality and other factors (Péron et al., 2017).

Description	Parameter	Prior
Vertical drift (altitude)	π_1	*Truncated Normal* (100, 45) [30,]
	π_2	- π_1
	π_3	*Truncated Normal* (40, 45) [30,]
	π_4	0
	π_5	0
Standard deviation (altitude)	σ_1	*Uniform* (0, 150)
	σ_2	σ_1
	σ_3	*Uniform* (0, 150)
	σ_4	10
	σ_5	*Uniform* (0, 150)
Concentration (turning angle)	ρ_1	*Uniform* (0.5, 1)
	ρ_2	ρ_1
	ρ_3	*Uniform* (0, ρ_1)
	ρ_4	*Uniform* (0, 0.5)
	ρ_5	ρ_1
Scale (step length)	$\log(\alpha_1)$	*Uniform* (-1, 7)
	$\log(\alpha_2)$	$\log(\alpha_1)$
	$\log(\alpha_3)$	*Uniform* (-1, $\log(\alpha_1)$)
	$\log(\alpha_4)$	*Uniform* (-1, $\log(\alpha_3)$)
	$\log(\alpha_5)$	*Uniform* (-1, $\log(\alpha_1)$)
Shape (step length)	$\log(\beta_1)$	*Uniform* (-1, 2)
	$\log(\beta_2)$	$\log(\beta_1)$
	$\log(\beta_3)$	*Uniform* (-1, 2)
	$\log(\beta_4)$	*Uniform* (-1, 2)
	$\log(\beta_5)$	*Uniform* (-1, 2)
Mean (hierarchical slope position)	κ_1	*Normal* (0.3, 0.3)
	κ_2	κ_1
	κ_3	κ_1
	κ_4	*Normal* (0.3, 0.3)
	κ_5	*Truncated Normal* (0.4, 0.3) [κ_1,]
Standard deviation (hierarchical slope position)	ω_1	*Uniform* (0, 0.2)
	ω_2	ω_1
	ω_3	ω_1
	ω_4	*Uniform* (0, 0.2)
	ω_5	*Uniform* (0, 0.2)
Transition probabilities from each state i	$\gamma_{i,1\ldots5}$	*Dirichlet* (1,1,1,1,1)
Initial state probabilities	$\varphi_{1\ldots5}$	*Dirichlet* (1,1,1,1,1)

Appendix S2. JAGS code for the model.

```
model
{

##Priors and constraints by state##

#Mean vertical drift
pi[1] ~ dnorm(100,0.0005)T(30,)
pi[2] <- -pi[1]
pi[3] ~ dnorm(40,0.0005)T(30,)
pi[4] <- 0
pi[5] <- 0

#STD vertical drift
sigma[1] ~ dunif(0,150)
sigma[2] <- sigma[1]
sigma[3] ~ dunif(0,150)
sigma[4] <- 10
sigma[5] ~ dunif(0,150)
for (i in 1:nstates){
 upsi.tau[i] <- 1/sigma[i]/sigma[i] #transform STD to precision
 }

#Concentration parameter for turning angle
rho[1] ~ dunif(0.5,1)
rho[2] <- rho[1]
rho[3] ~ dunif(0,rho[1])
rho[4]  ~ dunif(0,0.5)
```

```
rho[5] <- rho[1]

#Mean turning angle (fixed)
mu <- 0

#Parameters for step length distribution (on log scale)
logalpha[1] ~ dunif(-1,log.maxalpha)
logalpha[2] <- logalpha[1]
logalpha[3] ~ dunif(-1,logalpha[1])
logalpha[4] ~ dunif(-1,logalpha[3])
logalpha[5] ~ dunif(-1,logalpha[1])

logbeta[1] ~ dunif(-1,log.maxbeta)
logbeta[2] <- logbeta[1]
logbeta[3] ~ dunif(-1,log.maxbeta)
logbeta[4] ~ dunif(-1,log.maxbeta)
logbeta[5] ~ dunif(-1,log.maxbeta)

for (i in 1:nstates){
 alpha[i] <- exp(logalpha[i])
 beta[i] <- exp(logbeta[i])
 #JAGS uses different Weibull parameterization than R
 lambda[i] <- 1/pow(alpha[i],beta[i])
 }

#Mean HSP
kappa[1] ~ dnorm(0.3,10)
kappa[2] <- kappa[1]
kappa[3] <- kappa[1]
kappa[4] ~ dnorm(0.3,10)
```

```
kappa[5] ~ dnorm(0.4,10)T(kappa[1],)

#STD HSP
omega[1] ~ dunif(0,0.2)
omega[2] <- omega[1]
omega[3] <- omega[1]
omega[4] ~ dunif(0,0.2)
omega[5] ~ dunif(0,0.2)
for (i in 1:nstates){
 hsp.tau[i] <- 1/omega[i]/omega[i] #transform STD to precision
 }

#Initial state probabilities
phi[1:nstates] ~ ddirch(phiprior[1:nstates])

#Transition probabilities
for (i in 1:nstates){
 gamma[i,1:nstates] ~ ddirch(phiprior[1:nstates])
 }

#Observation error on altitude
epsilon <- 25
a.tau <- 1/epsilon/epsilon

##Model##
for (k in 1:ntracks){                              #loop over track segments
 s[Xidx[k]] ~ dcat(phi[1:nstates])                 #initial behavioural state
 upsilon[Xidx[k]+1] ~ dnorm(a[Xidx[k]+1], a.tau)       #initial true altitude

 #State proportions
```

```
state.cnt[1,Xidx[k]] <- equals(s[Xidx[k]],1)
state.cnt[2,Xidx[k]] <- equals(s[Xidx[k]],2)
state.cnt[3,Xidx[k]] <- equals(s[Xidx[k]],3)
state.cnt[4,Xidx[k]] <- equals(s[Xidx[k]],4)
state.cnt[5,Xidx[k]] <- equals(s[Xidx[k]],5)

for (t in (Xidx[k]+1):(Xidx[k+1]-2)){                  #loop over time steps
  s[t] ~ dcat(gamma[s[t-1],1:nstates])                 #behavioural state

  upsi.mean[t+1] <- upsilon[t] + pi[s[t]]              #mean altitude
  upsilon[t+1] ~ dnorm(upsi.mean[t+1], upsi.tau[s[t]])#process error (true altitude)
  a[t+1] ~ dnorm(upsilon[t+1], a.tau)                  #observed altitude (with
   observation error)

  h[t] ~ dnorm(kappa[b[t]], hsp.tau[b[t]])             #Hierarchical Slope Position

  x[t] ~ dweib(beta[s[t]],lambda[s[t]])                #step length

  #"ones" trick to sample from the Wrapped Cauchy distribution
  ones[t] ~ dbern(wC[t])
  wC[t] <- ( 1/(2*Pi)*(1-rho[s[t]]*rho[s[t]])/(1+rho[s[t]]*rho[s[t]]-
   2*rho[s[t]]*cos(theta[t]-mu)) )/500

  #State proportions
  state.cnt[1,t] <- equals(s[t],1)
  state.cnt[2,t] <- equals(s[t],2)
  state.cnt[3,t] <- equals(s[t],3)
  state.cnt[4,t] <- equals(s[t],4)
  state.cnt[5,t] <- equals(s[t],5)
```

```
   }#close temporal loop

  state.cnt[1,Xidx[k+1]-1]<-0
  state.cnt[2,Xidx[k+1]-1]<-0
  state.cnt[3,Xidx[k+1]-1]<-0
  state.cnt[4,Xidx[k+1]-1]<-0
  state.cnt[5,Xidx[k+1]-1]<-0

  }#close track loop

 #Monitor state convergence
 delta[1] <- sum(state.cnt[1,1:(Xidx[ntracks+1]-1)])/(Xidx[ntracks+1]-1-ntracks)
 delta[2] <- sum(state.cnt[2,1:(Xidx[ntracks+1]-1)])/(Xidx[ntracks+1]-1-ntracks)
 delta[3] <- sum(state.cnt[3,1:(Xidx[ntracks+1]-1)])/(Xidx[ntracks+1]-1-ntracks)
 delta[4] <- sum(state.cnt[4,1:(Xidx[ntracks+1]-1)])/(Xidx[ntracks+1]-1-ntracks)
 delta[5] <- sum(state.cnt[5,1:(Xidx[ntracks+1]-1)])/(Xidx[ntracks+1]-1-ntracks)

}
```

Table S3. Posterior estimates of model parameters (median and 95% highest posterior density interval). For each parameter, the table also reports the effective sample size and convergence diagnostics: upper confidence interval (CI) of the Brooks-Gelman-Rubin (BGR) diagnostic and percentage of Monte Carlo error (MCE) to sample standard deviation (SSD).

Description	Parameter	Lower (2.5%)	Median	Upper (97.5%)	Effective sample size	BGR diagnostic (upper CI)	% MCE/SSD
Vertical drift (altitude)	$\pi_1 = -\pi_2$	74	76	77	3315	1.01	1.74
	π_3	52	53	55	3509	1	1.69
Standard deviation (altitude)	$\sigma_1 = \sigma_2$	64	65	66	2527	1	2.10
	σ_3	71	72	74	2652	1	1.95
	σ_5	95	97	99	2621	1.01	1.96
Concentration (turning angle)	$\rho_1 = \rho_2 = \rho_5$	0.83	0.84	0.84	3874	1.01	1.63
	ρ_3	0.62	0.63	0.64	3552	1.01	1.69
	ρ_4	0.00	0.00	0.00	4286	1	1.53
Scale (step length)	$\alpha_1 = \alpha_2$	1058	1065	1071	1515	1	2.59
	α_3	385	390	395	1437	1	2.69
	α_4	22	23	24	1454	1.02	2.62
	α_5	654	663	672	2346	1	2.09
Shape (step length)	$\beta_1 = \beta_2$	3.56	3.61	3.67	2360	1	2.07
	β_3	1.87	1.90	1.92	3568	1.01	1.75
	β_4	0.90	0.93	0.96	1155	1.02	3.22
	β_5	1.80	1.83	1.87	2860	1	1.88
Mean	$\kappa_1 = \kappa_2 = \kappa_3$	0.326	0.327	0.328	942	1.03	3.29
	κ_4	0.375	0.378	0.380	3931	1.01	1.68

(hierarchical slope position)	κ_5	0.448	0.450	0.452	901	1.01	3.39
Standard deviation (hierarchical slope position)	$\omega_1 = \omega_2 = \omega_3$	0.049	0.050	0.050	1663	1.02	2.49
	ω_4	0.070	0.071	0.073	4045	1	1.58
	ω_5	0.052	0.053	0.054	3158	1.01	1.80
State proportions	δ_1	0.02	0.03	0.03	504	1.01	4.45
	δ_2	0.30	0.31	0.31	1421	1	2.74
	δ_3	0.37	0.37	0.38	691	1.03	3.82
	δ_4	0.09	0.09	0.10	523	1.05	4.47
	δ_5	0.20	0.20	0.21	430	1.05	4.86
Transition probabilities	$\gamma_{1,1}$	0.754	0.785	0.815	2785	1	1.90
	$\gamma_{2,1}$	0.012	0.015	0.018	1481	1.01	2.68
	$\gamma_{3,1}$	0.001	0.002	0.003	1650	1	2.64
	$\gamma_{4,1}$	0.000	0.000	0.001	4657	1	1.47
	$\gamma_{5,1}$	0.000	0.000	0.001	2867	1	1.89
	$\gamma_{1,2}$	0.169	0.199	0.229	2414	1	2.08
	$\gamma_{2,2}$	0.714	0.723	0.732	4500	1	1.49
	$\gamma_{3,2}$	0.172	0.179	0.186	4091	1	1.56
	$\gamma_{4,2}$	0.000	0.000	0.001	4500	1.01	1.49
	$\gamma_{5,2}$	0.058	0.064	0.070	3831	1	1.62
	$\gamma_{1,3}$	0.000	0.001	0.006	3571	1	1.67
	$\gamma_{2,3}$	0.214	0.223	0.231	4223	1	1.54
	$\gamma_{3,3}$	0.781	0.789	0.796	4153	1	1.55
	$\gamma_{4,3}$	0.029	0.035	0.042	3100	1.01	1.79
	$\gamma_{5,3}$	0.020	0.025	0.029	2982	1	1.84
	$\gamma_{1,4}$	0.000	0.001	0.003	4644	1.01	1.47
	$\gamma_{2,4}$	0.000	0.001	0.002	3772	1	1.64
	$\gamma_{3,4}$	0.010	0.012	0.014	3936	1.01	1.61
	$\gamma_{4,4}$	0.938	0.946	0.953	3647	1.02	1.65

	$\gamma_{5,4}$	0.016	0.019	0.022	3559	1	1.68
	$\gamma_{1,5}$	0.005	0.013	0.026	1897	1	2.37
	$\gamma_{2,5}$	0.034	0.038	0.042	2987	1.01	1.86
	$\gamma_{3,5}$	0.016	0.019	0.022	2668	1	1.98
	$\gamma_{4,5}$	0.014	0.018	0.024	2828	1.01	1.88
	$\gamma_{5,5}$	0.884	0.892	0.899	3598	1	1.67
Initial state probabilities	φ_1	0.005	0.019	0.041	1686	1	2.46
	φ_2	0.092	0.155	0.221	2946	1	1.85
	φ_3	0.378	0.447	0.514	3456	1.01	1.70
	φ_4	0.109	0.137	0.169	4029	1.01	1.58
	φ_5	0.198	0.238	0.286	3053	1.01	1.83

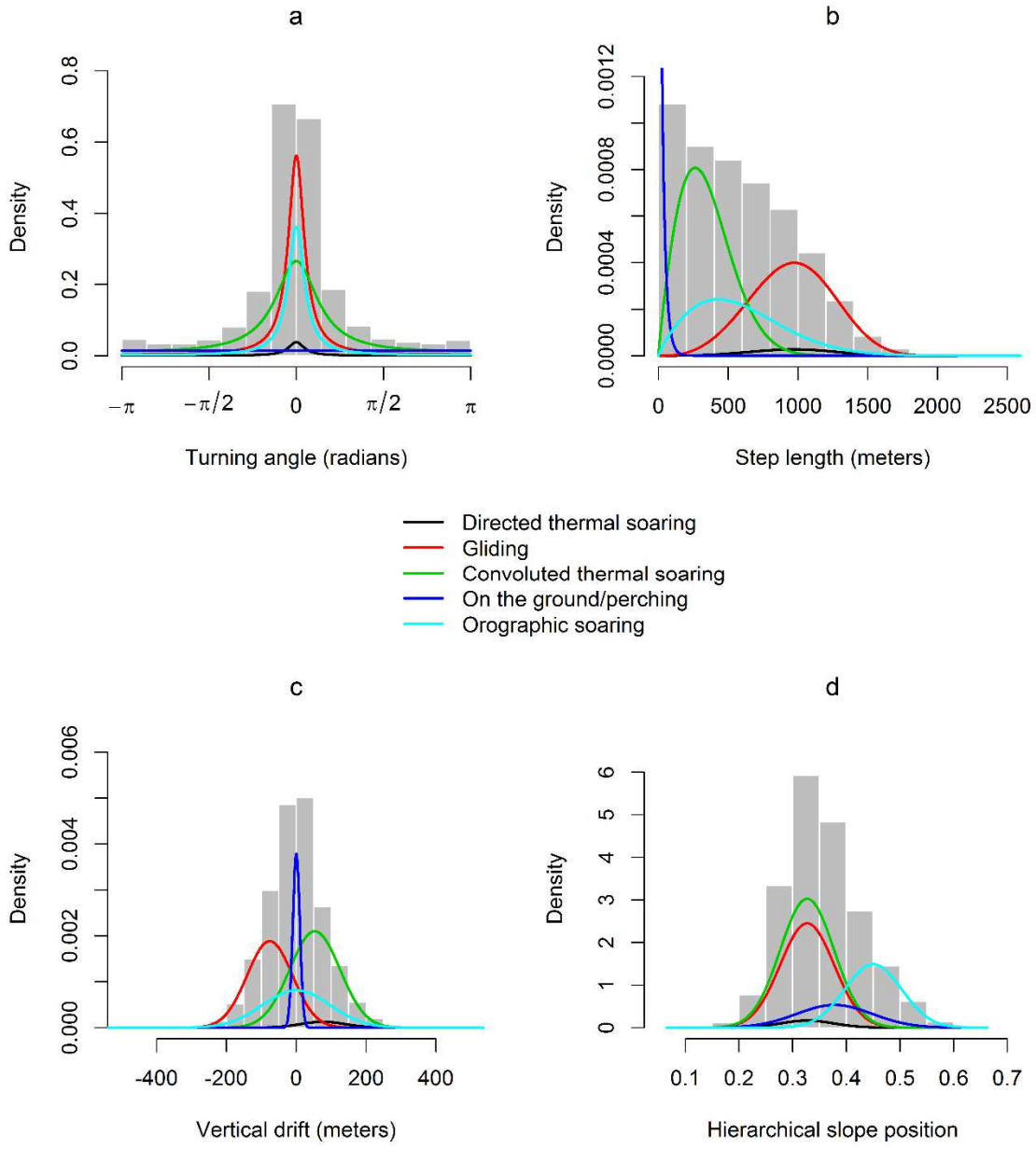


Figure S1. State-dependent emission distributions of the four response variables: a) turning angle, b) step length, c) vertical drift and d) hierarchical slope position, plotted over regularised data (grey histogram). To help visualisation, plots were truncated at 2000 m for step length and ±500 meters for vertical drift.

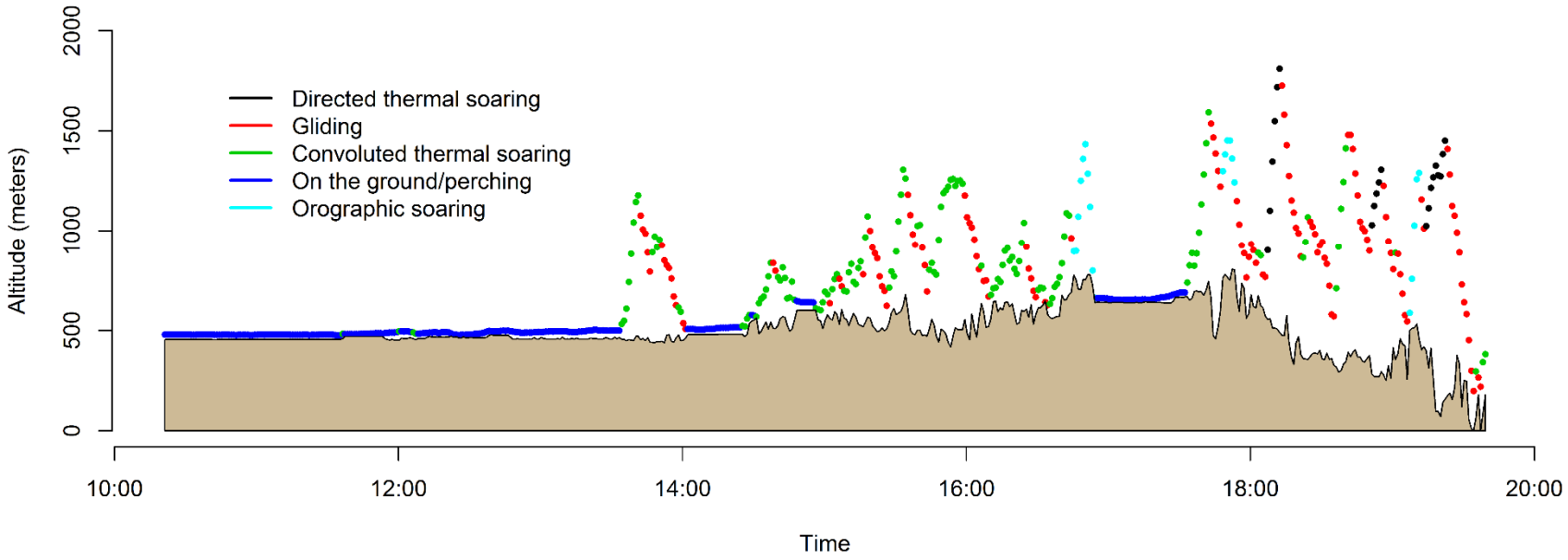


Figure S2. Example of time series of true altitudes from a track segment, coloured by the median posterior behavioural state at those locations. The filled polygon represents elevation at the corresponding GPS positions.

Table S4. Confusion matrix comparing manual state classifications (from Katzner et al., 2015) and model state estimates based on the posterior medians. Grey boxes highlight matching classifications.

Model → **↓ Manual**	*State 1 and 3 (thermal soaring)*	*State 2 (gliding)*	*State 5 (orographic soaring)*	*State 4 (on the ground or perching)*	**Accuracy**
Thermal soaring	1660	438	374	4	**0.67**
Gliding	446	1766	308	1	**0.70**
Orographic soaring	134	114	464	2	**0.65**
Unknown	1497	289	294	27	-
Reliability	**0.44**	**0.68**	**0.32**	-	

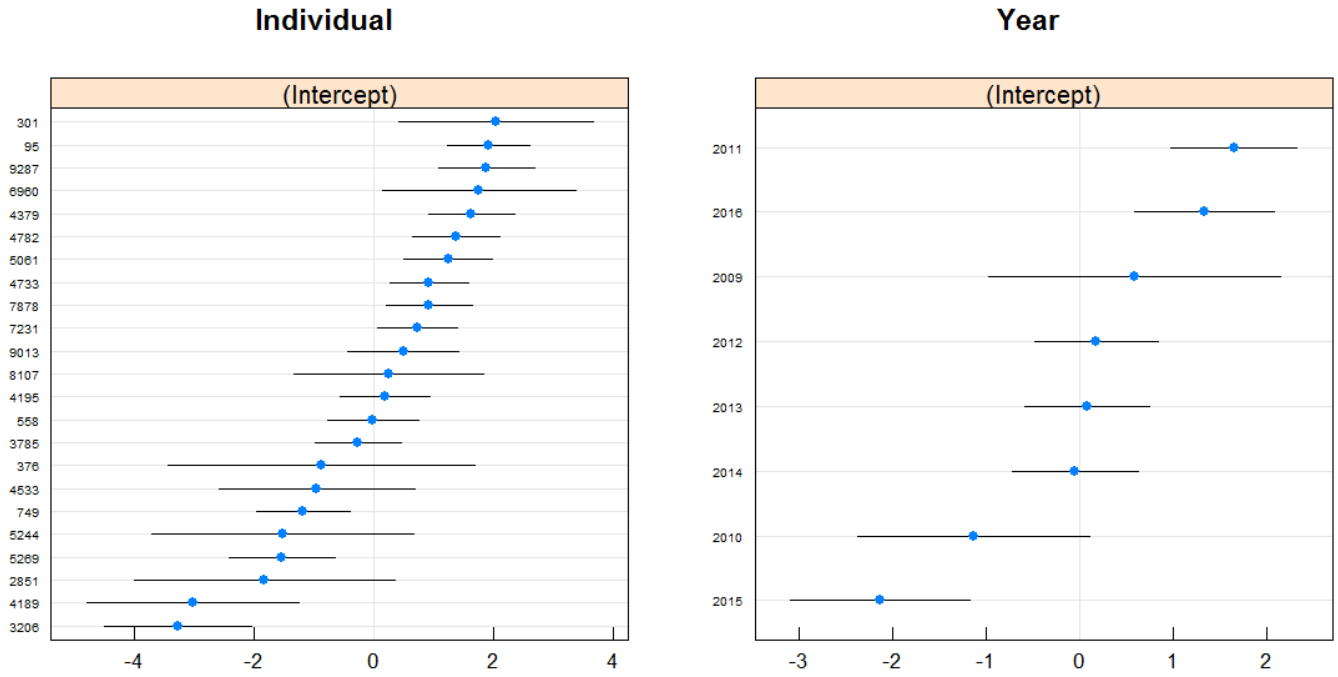
Table S5. Results of model selection for the behavioural models, based on Akaike's information criterion corrected by small samples sizes (AICc). Best models (i.e. minimising the AICc) are highlighted in bold. The symbol '*' indicates the interaction between two variables.

Behavioural state	*Data subset*	*Fixed effects*	*Random effects*	*AICc*
Directed thermal soaring (State 1)	Adults and sub-adults; autumn and spring	~ Season * Age	Individual	772
			Year	902
			Individual, Year	548
		~ Season + Age	**Individual, Year**	**546**
		~ Season	Individual, Year	567
		~ Age	Individual, Year	672
	Adults; autumn and spring	~ Season * Sex	Individual	324
			Year	473
			Individual, Year	288
		~ Season + Sex	Individual, Year	288
		~ Season	**Individual, Year**	**285**
		~ Sex	Individual, Year	352
Gliding (State 2)	Adults and sub-adults; autumn and spring	~ Season * Age	Individual	961
			Year	1066
			Individual, Year	858
		~ Season + Age	**Individual, Year**	**856**
		~ Season	Individual, Year	858
		~ Age	Individual, Year	1041
	Adults; autumn and spring	**~ Season * Sex**	Individual	448
			Year	577
			Individual, Year	**411**
		~ Season + Sex	Individual, Year	462
Convoluted thermal soaring (State 3)	Adults and sub-adults; autumn and spring	**~ Season * Age**	Individual	854
			Year	1196
			Individual, Year	**805**
		~ Season + Age	Individual, Year	817
	Adults; autumn and spring	~ Season * Sex	Individual	457
			Year	606
			Individual, Year	460

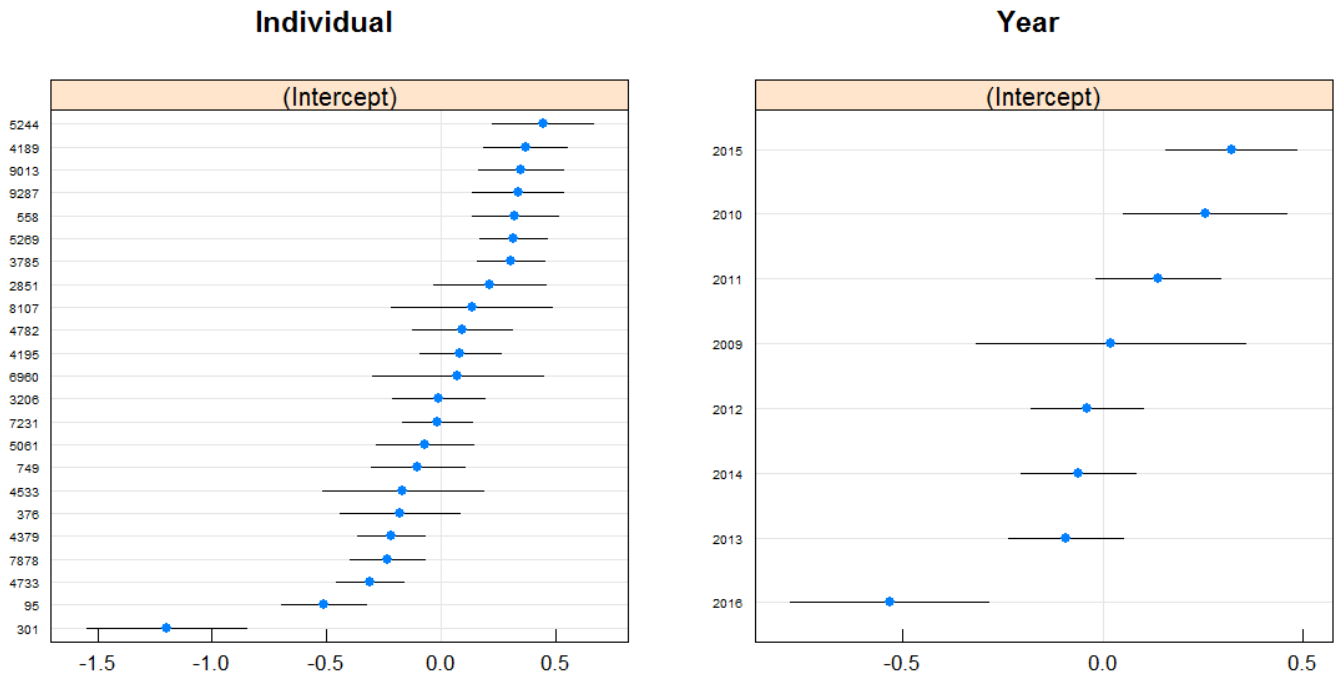
		~ Season + Sex	Individual	455
		~ Season	**Individual**	**453**
		~ Sex	Individual	460
Orographic soaring (State 5)	Adults and sub-adults; autumn and spring	~ Season * Age	Individual	1548
			Year	1913
			Individual, Year	1364
		~ Season + Age	**Individual, Year**	**1362**
		~ Season	Individual, Year	1423
		~ Age	Individual, Year	1524
	Adults; autumn and spring	**~ Season * Sex**	Individual	773
			Year	859
			Individual, Year	**711**
		~ Season + Sex	Individual, Year	821

Figure S3. Dot plots of the random effects of individual and year in the final behavioural models. a-d) Results of the models assessing age and seasonal differences in the proportional occurrence of directed thermal soaring, convoluted thermal soaring, gliding and orographic soaring, respectively. f-e) Results of the models assessing sex and seasonal differences in the proportional occurrence of gliding and orographic soaring, respectively. All random effects are reported on the link scale (logit).

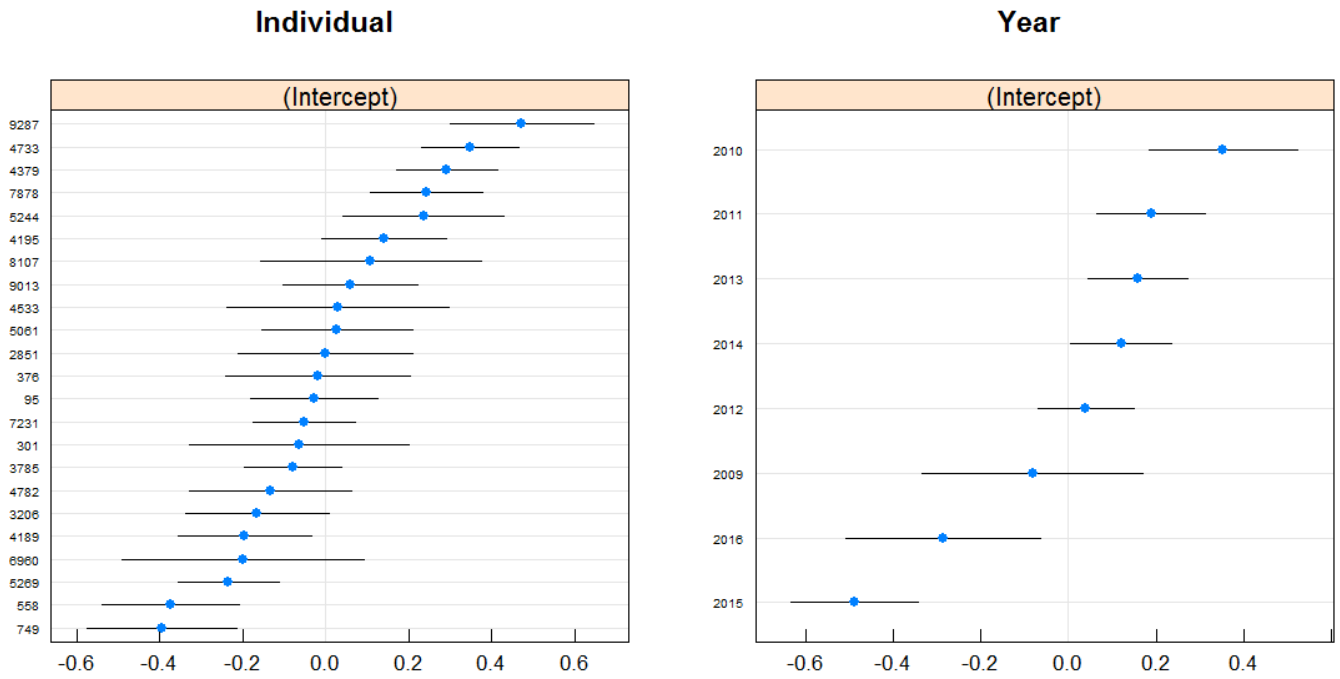
a)



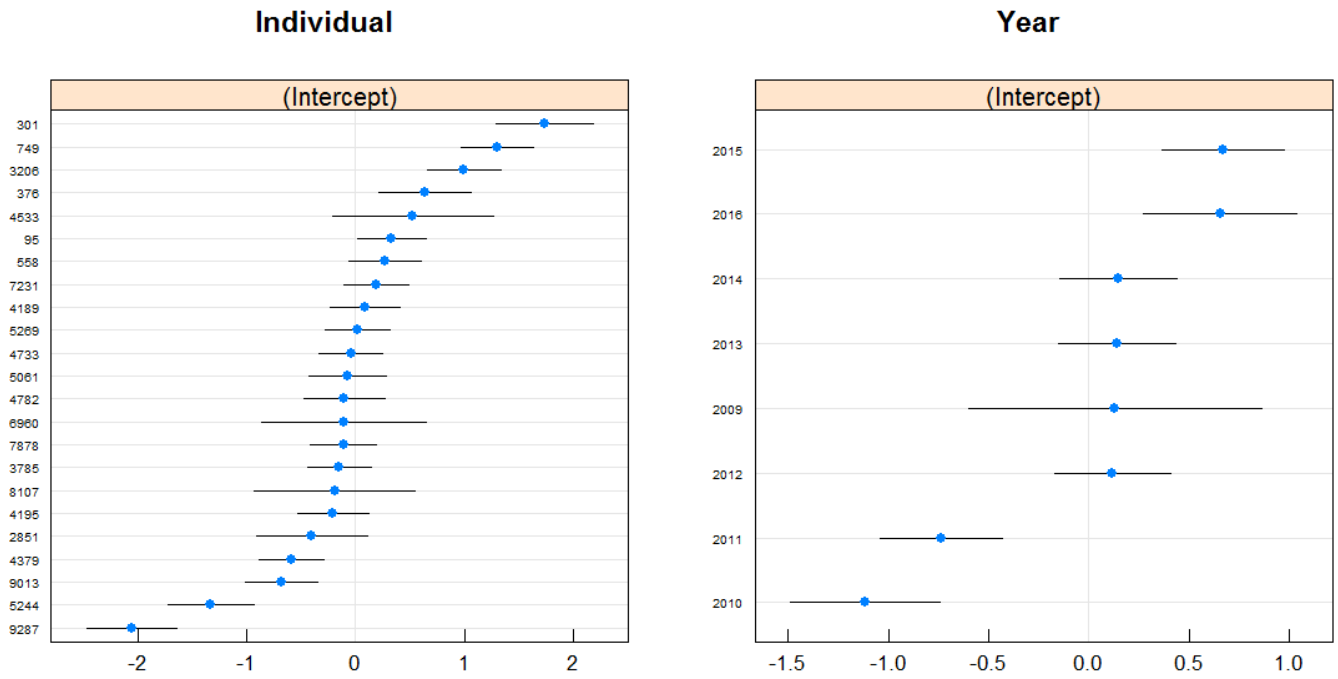
b)


Individual
(Intercept)
5244
4189
9013
9287
558
5269
3785
2851
8107
4782
4195
6960
3206
7231
5061
749
4533
376
4379
7878
4733
95
301
-1.5
-1.0
-0.5
0.0
0.5
Year
(Intercept)
2015
2010
2011
2009
2012
2014
2013
2016
-0.5
0.0
0.5

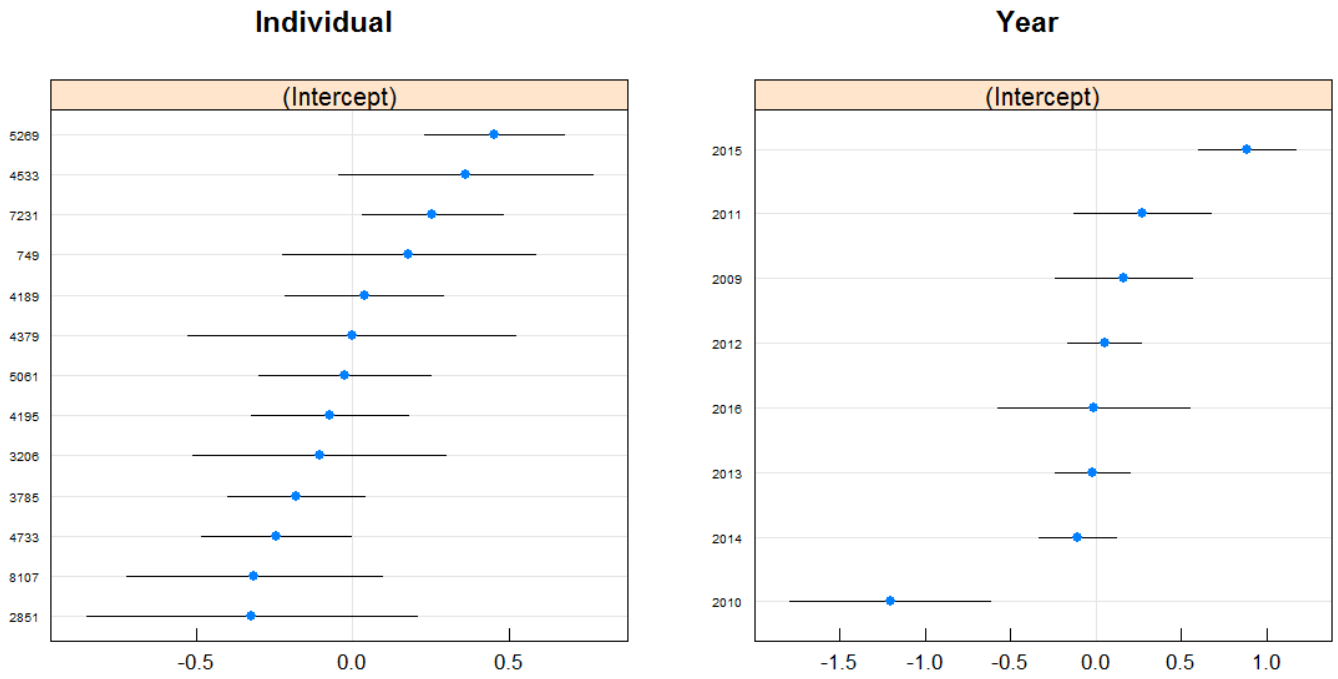
c)


Individual
(Intercept)
9287
4733
4379
7878
5244
4195
8107
9013
4533
5061
2851
376
95
7231
301
3785
4782
3206
4189
6960
5269
558
749
-0.6
-0.4
-0.2
0.0
0.2
0.4
0.6
Year
(Intercept)
2010
2011
2013
2014
2012
2009
2016
2015
-0.6
-0.4
-0.2
0.0
0.2
0.4

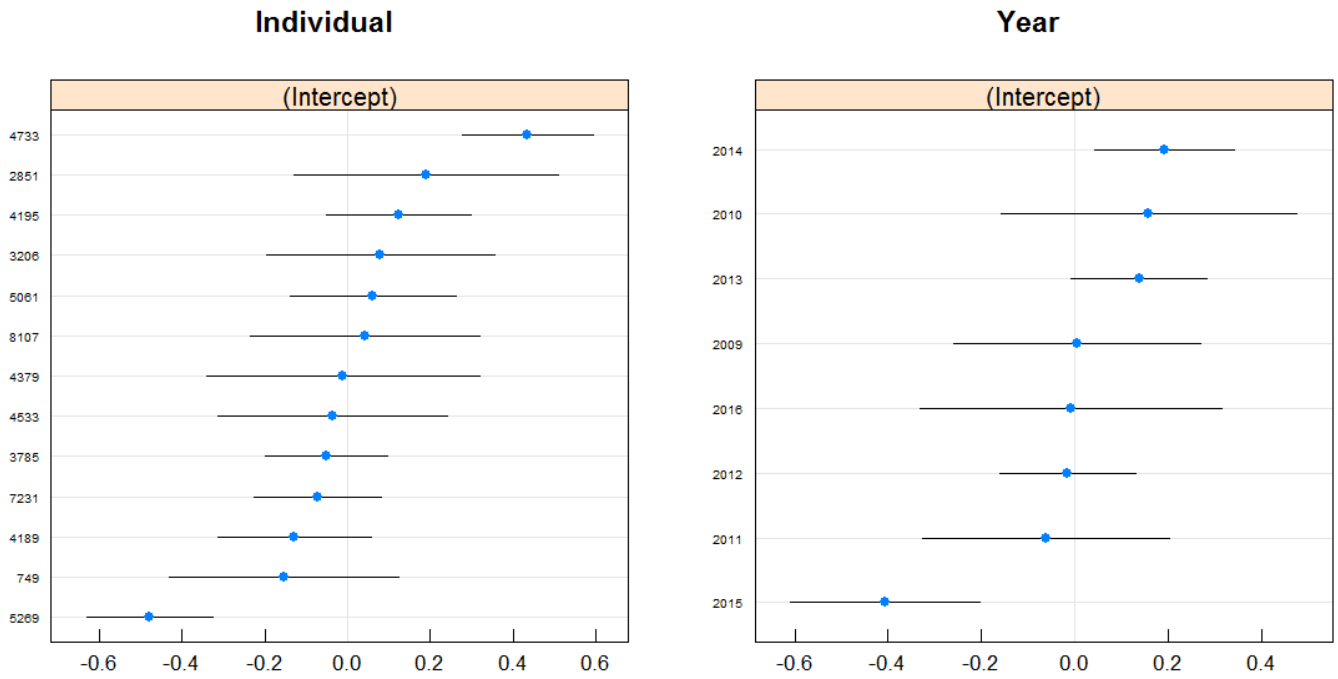
d)


Individual
(Intercept)
301
749
3206
376
4533
95
558
7231
4189
5269
4733
5061
4782
6960
7878
3785
8107
4195
2851
4379
9013
5244
9287
-2
-1
0
1
2
Year
(Intercept)
2015
2016
2014
2013
2009
2012
2011
2010
-1.5
-1.0
-0.5
0.0
0.5
1.0

e)


Individual
(Intercept)
5269
4533
7231
749
4189
4379
5061
4195
3206
3785
4733
8107
2851
-0.5
0.0
0.5
Year
(Intercept)
2015
2011
2009
2012
2016
2013
2014
2010
-1.5
-1.0
-0.5
0.0
0.5
1.0

f)


Individual
(Intercept)
4733
2851
4195
3206
5061
8107
4379
4533
3785
7231
4189
749
5269
-0.6
-0.4
-0.2
0.0
0.2
0.4
0.6
Year
(Intercept)
2014
2010
2013
2009
2016
2012
2011
2015
-0.6
-0.4
-0.2
0.0
0.2
0.4

Appendix S3. Reformulation of the model allowing for missing data.

The interpolation procedure used to fill any remaining, short (≤5 min) gaps in the observed track segments may introduce errors in the time series of response variables, particularly in the horizontal dimension. To test whether model results were affected by interpolated observations over these short gaps, the model was reformulated to allow for missing data points in the response variables. Specifically, whenever the time interval between a regularised location and the closest observed location was greater than 1 minute, rather than using the interpolated values of the response variables, the model was asked to estimate the missing values of the response variables, together with the rest of the parameters. When altitude information was missing at the second location of a segment (affecting the estimation of the vertical drift at the first location), a truncated Gaussian prior was provided, centred on the mean altitude for the corresponding segment, with a standard deviation of 2,000 m and truncation at the extremes of the observed altitude range.

The estimates of the parameters and associated uncertainty from this alternative version of the model are reported below. The 95% highest posterior density intervals for all parameters were largely overlapping between the two model formulations. As a result, the proportion of minutes classified under each latent state ($\delta_{1,\ldots,5}$) also remained largely unchanged in the new formulation.

Description	Parameter	Lower (2.5%)	Median	Upper (97.5%)
Vertical drift (altitude)	$\pi_1 = -\pi_2$	75	76	78
	π_3	52	53	55
Standard deviation (altitude)	$\sigma_1 = \sigma_2$	64	65	66
	σ_3	72	73	74
	σ_5	93	95	97
Concentration (turning angle)	$\rho_1 = \rho_2 = \rho_5$	0.83	0.83	0.83
	ρ_3	0.62	0.63	0.64
	ρ_4	0.00	0.00	0.00
Scale (step length)	$\alpha_1 = \alpha_2$	1061	1068	1075
	α_3	386	391	396
	α_4	22	23	24
	α_5	655	664	673
Shape (step length)	$\beta_1 = \beta_2$	3.57	3.62	3.68
	β_3	1.86	1.89	1.92
	β_4	0.90	0.92	0.95
	β_5	1.79	1.83	1.86
Mean (hierarchical slope position)	$\kappa_1 = \kappa_2 = \kappa_3$	0.326	0.327	0.328
	κ_4	0.376	0.378	0.380
	κ_5	0.448	0.450	0.451
Standard deviation (hierarchical slope position)	$\omega_1 = \omega_2 = \omega_3$	0.049	0.050	0.050
	ω_4	0.070	0.071	0.073
	ω_5	0.052	0.053	0.054
State proportions	δ_1	0.02	0.03	0.03
	δ_2	0.30	0.30	0.31
	δ_3	0.37	0.37	0.38
	δ_4	0.09	0.09	0.10
	δ_5	0.20	0.20	0.21
Transition probabilities	$\gamma_{1,1}$	0.752	0.784	0.814
	$\gamma_{2,1}$	0.012	0.015	0.018
	$\gamma_{3,1}$	0.001	0.002	0.003
	$\gamma_{4,1}$	0.000	0.000	0.001
	$\gamma_{5,1}$	0.000	0.000	0.001
	$\gamma_{1,2}$	0.170	0.200	0.232
	$\gamma_{2,2}$	0.711	0.720	0.729
	$\gamma_{3,2}$	0.174	0.181	0.188
	$\gamma_{4,2}$	0.000	0.000	0.001

	$\gamma_{5,2}$	0.058	0.064	0.071
	$\gamma_{1,3}$	0.000	0.001	0.006
	$\gamma_{2,3}$	0.217	0.225	0.234
	$\gamma_{3,3}$	0.779	0.787	0.795
	$\gamma_{4,3}$	0.029	0.035	0.043
	$\gamma_{5,3}$	0.020	0.024	0.029
	$\gamma_{1,4}$	0.000	0.001	0.004
	$\gamma_{2,4}$	0.000	0.001	0.002
	$\gamma_{3,4}$	0.010	0.012	0.014
	$\gamma_{4,4}$	0.937	0.945	0.952
	$\gamma_{5,4}$	0.016	0.019	0.022
	$\gamma_{1,5}$	0.004	0.013	0.026
	$\gamma_{2,5}$	0.034	0.039	0.043
	$\gamma_{3,5}$	0.015	0.018	0.021
	$\gamma_{4,5}$	0.014	0.019	0.024
	$\gamma_{5,5}$	0.885	0.892	0.899
Initial state probabilities	φ_1	0.005	0.020	0.042
	φ_2	0.089	0.153	0.222
	φ_3	0.381	0.452	0.519
	φ_4	0.102	0.132	0.164
	φ_5	0.197	0.241	0.287

Appendix S4. Analysis of simulated data.

In order to investigate whether irregular sampling (resulting in gaps in the tracking data) and measurement errors in the vertical and horizontal dimensions affected the ability of the model to estimate the parameters correctly, we explored the performance of the model by means of simulated data.

First, the posterior estimates of the parameters of the state-dependent emission distributions and of the transition probabilities were used to simulate thirty 10,000-minute-long time series of step length, turning angle, altitude and hierarchical slope position values. Specifically, the initial behavioural state for each track was set to 4 (i.e. on the ground or perching). A random value was then drawn from the posterior distribution of each parameter of the state-dependent emission distributions and of the corresponding transition probabilities. The set of transition probabilities was used to draw the behavioural state in the following time step, while the emission distributions were used to simulate a new value for each response variable. This was repeated 10,000 times for each simulated track. Errors in the vertical dimension were simulated using the same observation model used in the original analysis. We then extracted all gaps ≥2 min observed in the original data and distributed them randomly over the simulated data. Very large gaps (≥1 d) were excluded because they could not be placed randomly over the simulated tracks without generating extremely large tracks; however, this is unlikely to affect the outcome of the simulation procedure, because larger gaps would simply lead to the creation of additional segments. As described in the data processing section, we then divided tracks into separate segments whenever the gap was greater than 5 min, and interpolated the values of the response variables for shorter gaps. The first 7,000 observations of each track were discarded to: 1) avoid any influence of initial conditions; and 2) obtain a simulated tracking dataset of comparable size

to the original data. The final simulated dataset included 42,783 data points. We simulated errors in the horizontal dimension using a randomly sampled HDOP value from the original dataset: we drew a random value from a Gaussian distribution centred on the simulated step length, with standard deviation equal to the random HDOP value multiplied by the GPS error of the devices (3 m). Finally, we ran the state-space analysis on the resulting, simulated data, using the same priors and initial values as in the original analysis.

The estimates of the parameters and associated uncertainty from the analysis of the simulated data are reported below. With the exception of the initial state probabilities (which are necessarily different in the simulated data) and, to a certain extent, of the state proportions (reflecting the simulation ability of the model; see discussion in Appendix S5), the 95% highest posterior density intervals for all other parameters were largely overlapping between the analysis of observed and simulated data. These results suggest that the model is able to retrieve the correct parameter estimates despite observed gaps in the tracks and measurement errors.

Description	Parameter	Lower (2.5%)	Median	Upper (97.5%)
Vertical drift (altitude)	$\pi_1 = -\pi_2$	73	75	76
	π_3	51	53	54
Standard deviation (altitude)	$\sigma_1 = \sigma_2$	62	63	64
	σ_3	70	71	72
	σ_5	96	98	100
Concentration (turning angle)	$\rho_1 = \rho_2 = \rho_5$	0.83	0.84	0.84
	ρ_3	0.64	0.65	0.65
	ρ_4	0.00	0.01	0.02
Scale (step length)	$\alpha_1 = \alpha_2$	1055	1061	1067
	α_3	387	391	395
	α_4	24	25	25
	α_5	652	661	670
Shape (step length)	$\beta_1 = \beta_2$	3.57	3.63	3.68
	β_3	1.86	1.89	1.92
	β_4	0.96	0.98	1.00
	β_5	1.81	1.84	1.87
Mean (hierarchical slope position)	$\kappa_1 = \kappa_2 = \kappa_3$	0.326	0.327	0.327
	κ_4	0.375	0.377	0.379
	κ_5	0.449	0.450	0.451
Standard deviation (hierarchical slope position)	$\omega_1 = \omega_2 = \omega_3$	0.050	0.050	0.051
	ω_4	0.069	0.071	0.072
	ω_5	0.052	0.052	0.053
State proportions	δ_1	0.02	0.02	0.02
	δ_2	0.29	0.29	0.30
	δ_3	0.35	0.36	0.36
	δ_4	0.15	0.15	0.15
	δ_5	0.18	0.18	0.18
Transition probabilities	$\gamma_{1,1}$	0.702	0.741	0.778
	$\gamma_{2,1}$	0.014	0.018	0.021
	$\gamma_{3,1}$	0.001	0.003	0.004
	$\gamma_{4,1}$	0.000	0.000	0.001
	$\gamma_{5,1}$	0.000	0.001	0.003
	$\gamma_{1,2}$	0.190	0.226	0.265
	$\gamma_{2,2}$	0.711	0.721	0.730
	$\gamma_{3,2}$	0.171	0.178	0.186
	$\gamma_{4,2}$	0.000	0.001	0.003
	$\gamma_{5,2}$	0.059	0.065	0.072
	$\gamma_{1,3}$	0.000	0.005	0.020

	$\gamma_{2,3}$	0.216	0.224	0.233
	$\gamma_{3,3}$	0.782	0.789	0.797
	$\gamma_{4,3}$	0.032	0.037	0.042
	$\gamma_{5,3}$	0.020	0.025	0.030
	$\gamma_{1,4}$	0.000	0.001	0.007
	$\gamma_{2,4}$	0.001	0.001	0.002
	$\gamma_{3,4}$	0.011	0.013	0.015
	$\gamma_{4,4}$	0.937	0.943	0.949
	$\gamma_{5,4}$	0.016	0.019	0.023
	$\gamma_{1,5}$	0.013	0.025	0.041
	$\gamma_{2,5}$	0.032	0.036	0.040
	$\gamma_{3,5}$	0.014	0.017	0.019
	$\gamma_{4,5}$	0.015	0.019	0.023
	$\gamma_{5,5}$	0.881	0.889	0.897
Initial state probabilities	φ_1	0.006	0.010	0.032
	φ_2	0.254	0.323	0.398
	φ_3	0.276	0.346	0.417
	φ_4	0.100	0.128	0.159
	φ_5	0.154	0.191	0.233

Appendix S5. Posterior predictive checks.

Assessing the goodness-of-fit of hidden state models fitted in a Bayesian framework is less straightforward than in comparable frequentist models (Jonsen et al., 2013). Alternatively, posterior predictive checks can be used to assess the ability of the model to replicate various features of the observed data. De Haan-Rietdijk et al. (2017), Morales, Haydon, Frair, Holsinger, & Fryxell (2004), and Shirley, Small, Lynch, Maisto, & Oslin (2010) proposed several procedures to this purpose, which all aim to evaluate whether the simulation of new data using the posterior estimates of model parameters can generate summary statistics that are comparable with the same summary statistics in the empirical dataset.

We followed the procedure described in Appendix S4 to simulate 1,000 new datasets of comparable size based on random draws from the posterior distribution of the state-dependent parameters of the emission distributions and transition probabilities. By doing so, we implicitly accounted for uncertainty in these parameters. Results of the simulations were then compared to the dataset of filtered and regularised locations that was used to fit the model.

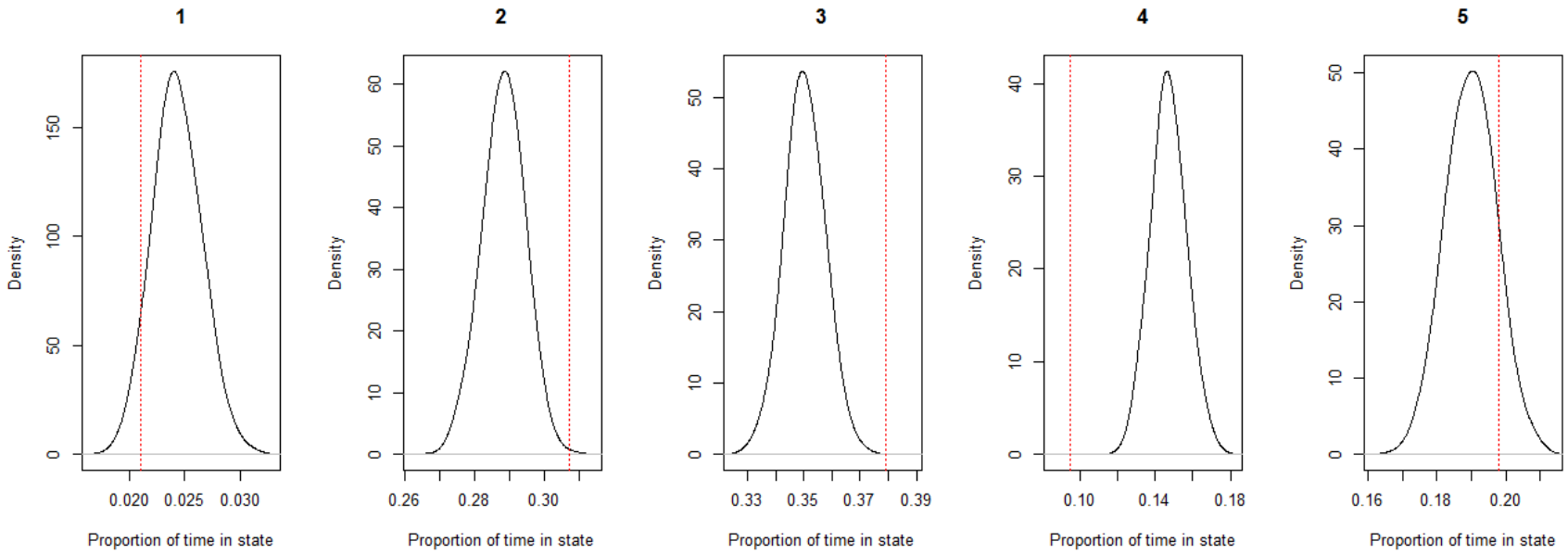
First, we compared the activity budget, i.e., the proportion of time spent in each latent state across all segments and tracks. The proportion of time spent in each state in the original data was plotted over the distribution of proportions obtained in the simulated datasets. Similarly, we calculated the mean and standard deviation of the duration of stays (i.e., the number of consecutive one-minute steps) in each state for each simulated dataset, and compared their distribution with the same statistics in the original data. We then considered the number of behavioural transitions per segment, corrected by the length of each segment. As for the previous metric, we plotted the mean and standard deviation in the original dataset over the distribution of the same statistics in the simulated dataset. Because the distributions of relative number of

behavioural transitions were not Gaussian and, therefore, the mean and standard deviation did not necessarily provide appropriate summaries as for the other metrics, we also plotted them together to verify their degree of overlap. Finally, we plotted the autocorrelation function plot (ACF) for all response variables in the original and simulated data.

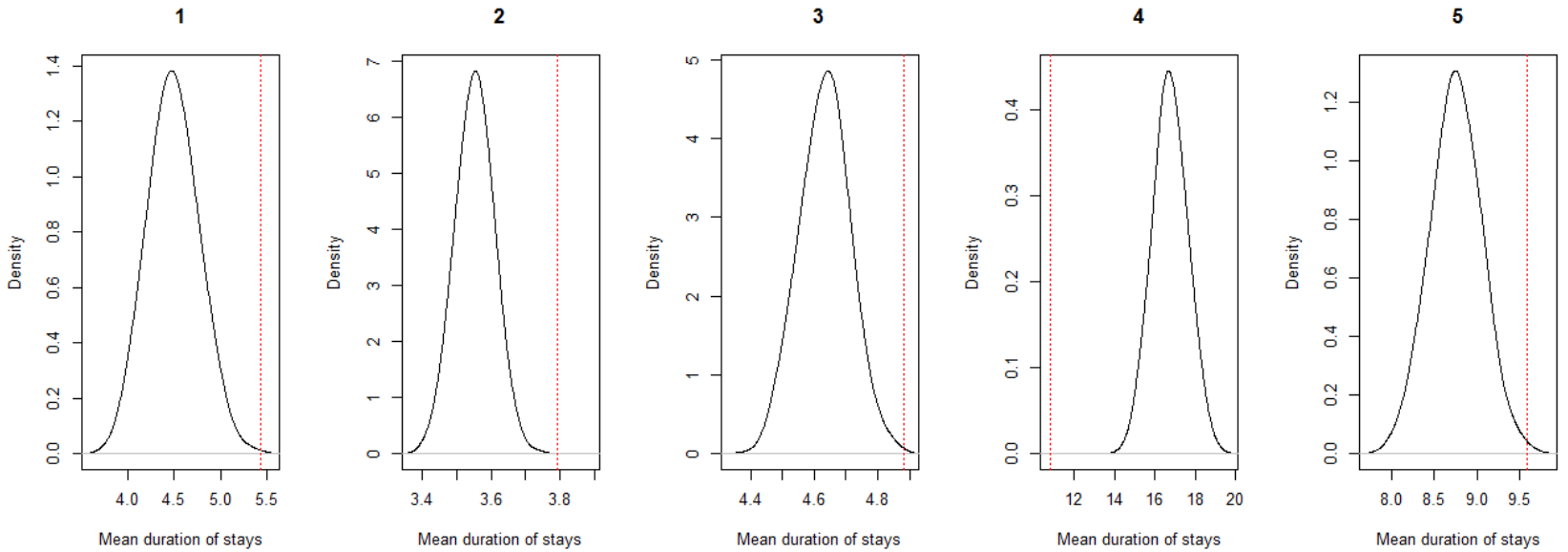
The activity budget estimated from the simulated data was, overall, satisfactorily comparable with the activity budget in the original data (Fig. S4a). In the simulated tracks, eagles allocated more time than expected to state 4 (on the ground or perching), which also partially affected the proportional occurrence of other states. However, this could result from the fact that, at night or when not flying (that is, when an eagle is most likely to spend time in this state), the GPS device was programmed to record location data less frequently, resulting in a higher chance of gap occurrence; on the other hand, gaps were distributed randomly in the simulated data. This is also reflected in the higher mean duration of stays in this state in the simulated data (Fig. S4b). For all other states, the mean duration of stays in the original data was higher than in the simulated data, highlighting the potential problems with the validity of the Markov property for the short time interval that are discussed in the main text (Fig. S4b and c). Similarly, the relative number of behavioural transitions per segment was slightly higher in the simulated data (Fig. S4d). As demonstrated in the overlap between the two distributions, this reflects a lower occurrence of intermediate numbers of transitions, which could characterise longer stretches of tracks spent in given states. Finally, the ACF plots confirmed these patterns and highlighted the occurrence of residual autocorrelation in some response variables (particularly step length and hierarchical slope position) under specific states (Fig. S5).

Figure S4. Results of the posterior predictive checks. In all plots, the dashed red line indicates the value of the corresponding metric in the original data, while the black line reports the kernel density of the same metric across 1,000 simulated datasets. a) Activity budget, expressed as the proportion of time spent in each behavioural state (1-5); b) mean duration of stays (i.e., the number of consecutive one-minute steps) per state; c) standard deviation of the duration of stays per state; d) mean, standard deviation and overall kernel density (black: simulated data; red: original data) of the number of behavioural transitions per segment, corrected by the length of each segment.

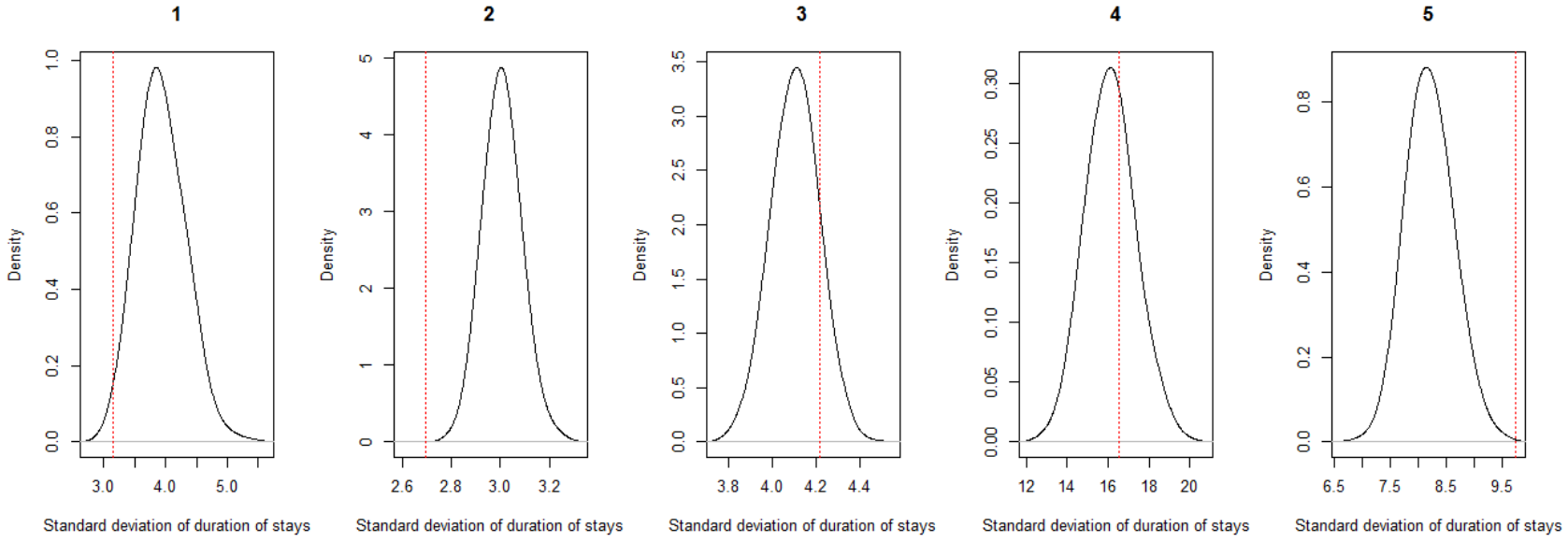
a)



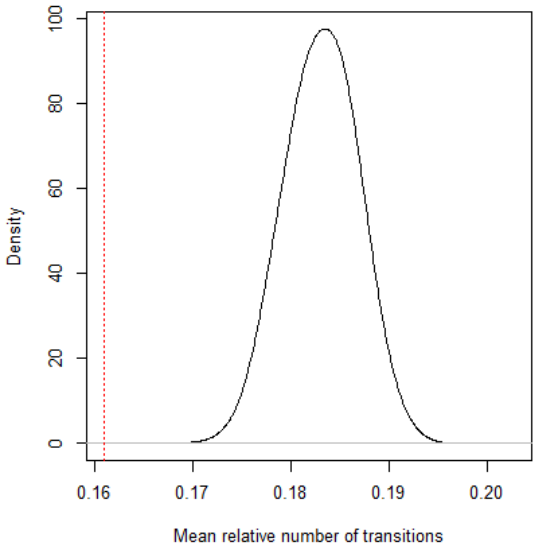
b)

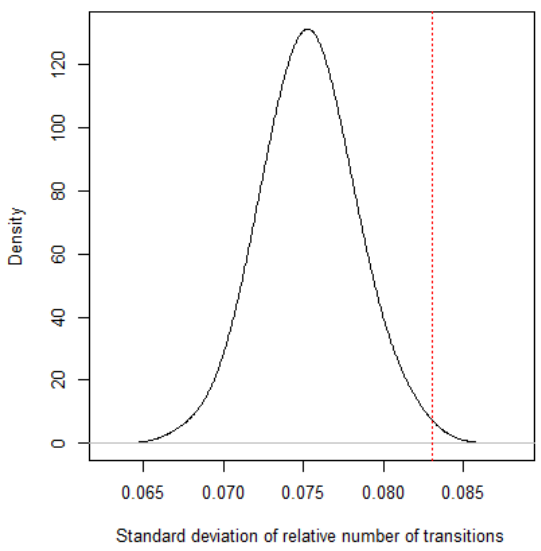

1
2
3
4
5
Density
Mean duration of stays

c)


1
2
3
4
5
Density
Standard deviation of duration of stays

d)


Density
0
20
40
60
80
100
0.16
0.17
0.18
0.19
0.20
Mean relative number of transitions


Density
0
20
40
60
80
100
120
0.065
0.070
0.075
0.080
0.085
Standard deviation of relative number of transitions

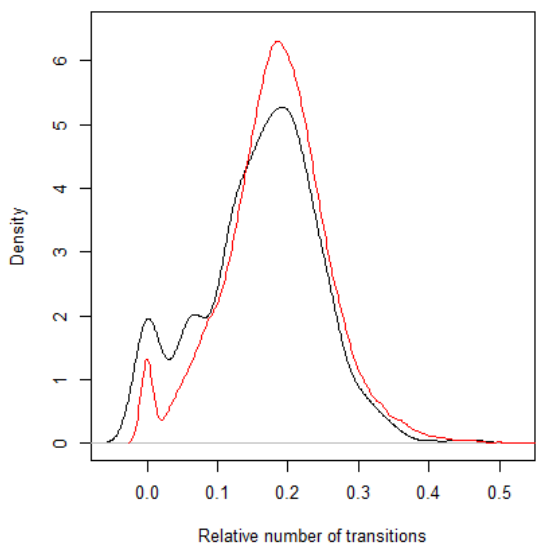
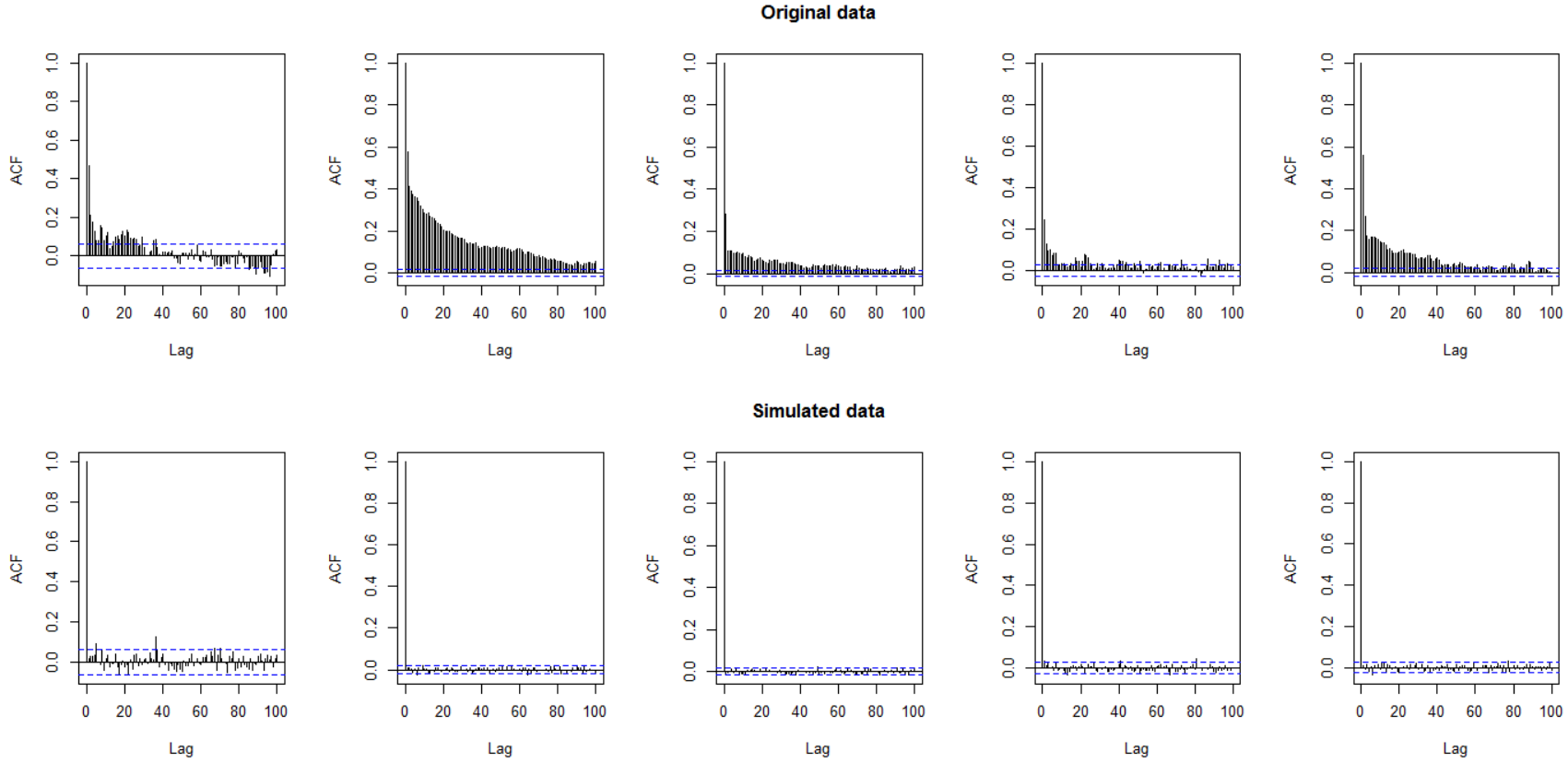
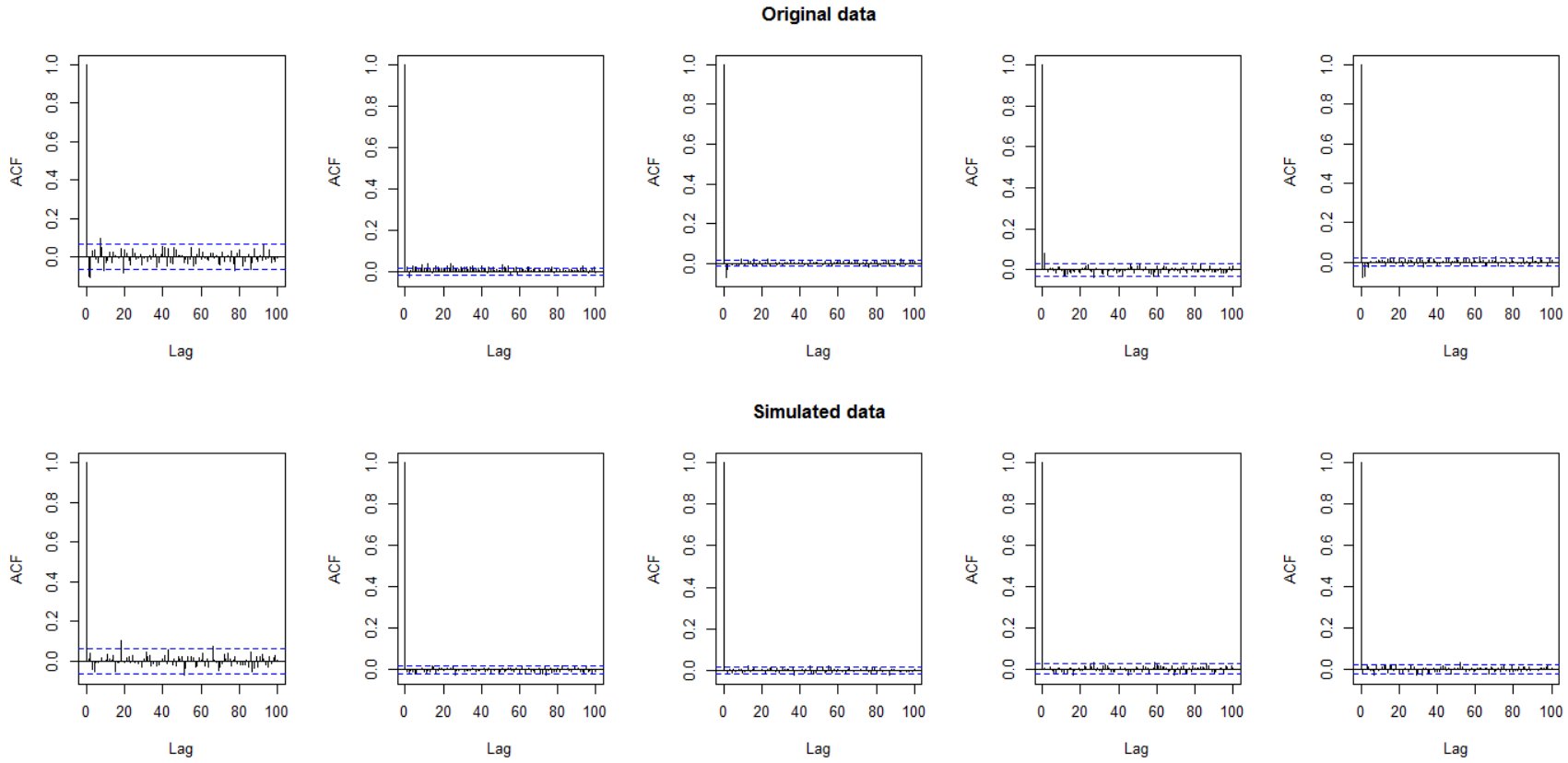

Density
0
1
2
3
4
5
6
0.0
0.1
0.2
0.3
0.4
0.5
Relative number of transitions

Figure S5. Autocorrelation function (ACF) plots for the response variables by state in the original and simulated data. a) Step length, b) turning angle, c) hierarchical slope position and d) vertical drift.

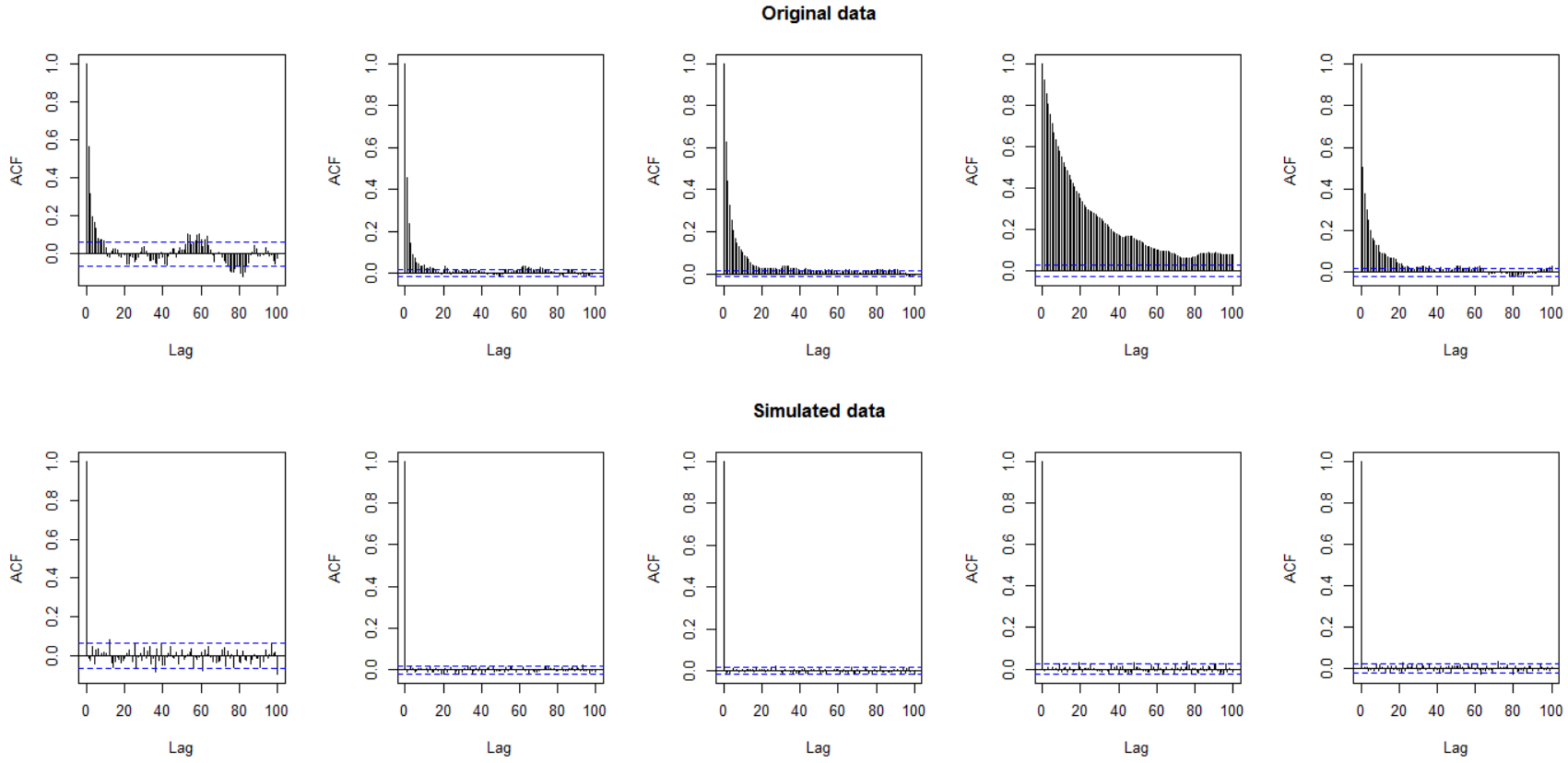
a)



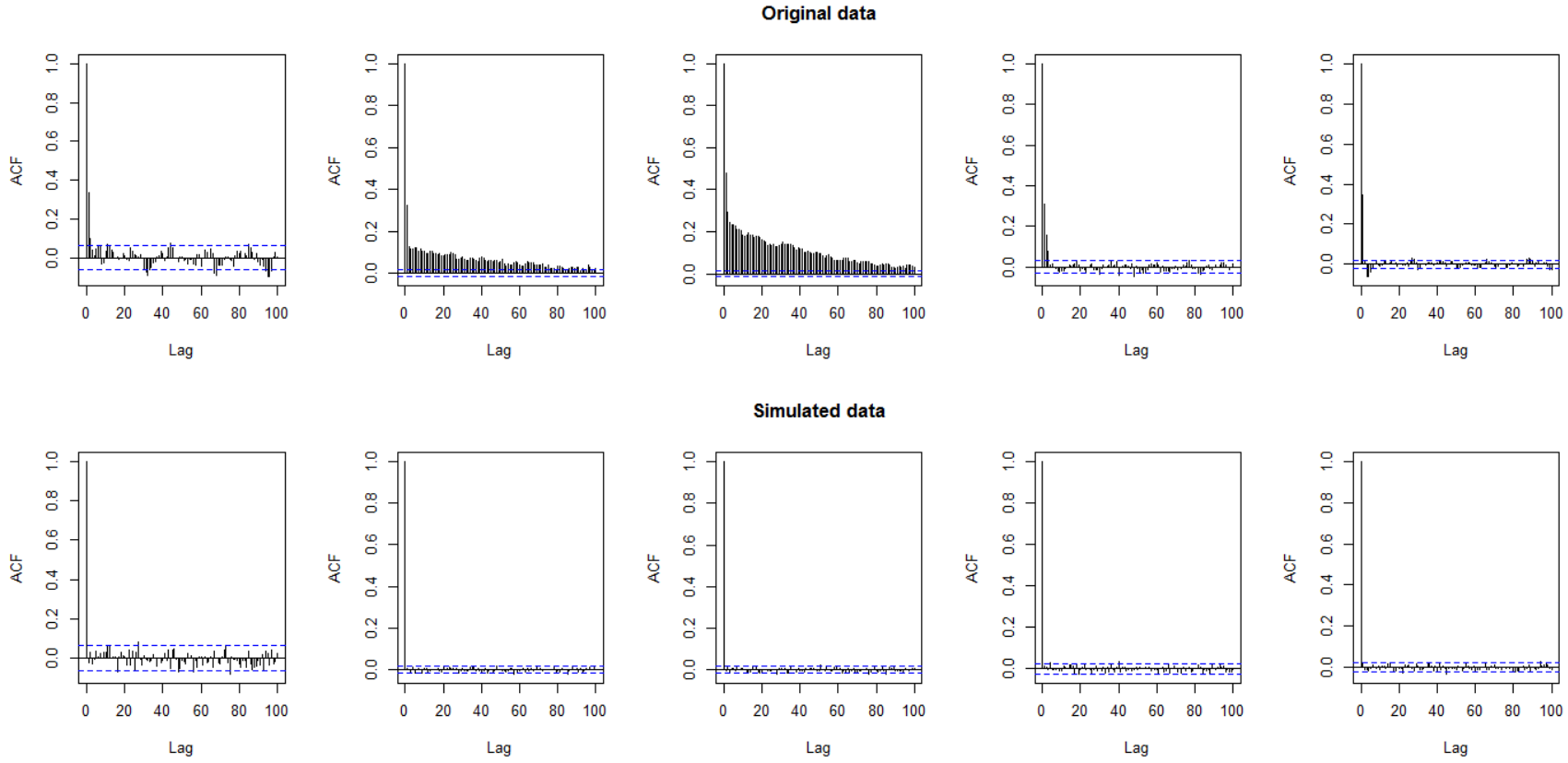
b)


Original data
Simulated data
ACF
Lag
0.0
0.2
0.4
0.6
0.8
1.0
0
20
40
60
80
100

c)


Original data
Simulated data
ACF
Lag
0.0
0.2
0.4
0.6
0.8
1.0
0
20
40
60
80
100

d)


Original data
Simulated data
ACF
Lag
0.0
0.2
0.4
0.6
0.8
1.0
0
20
40
60
80
100

References

de Haan-Rietdijk, S., Kuppens, P., Bergeman, C. S., Sheeber, L. B., Allen, N. B., & Hamaker, E. L. (2017). On the Use of Mixed Markov Models for Intensive Longitudinal Data. *Multivariate Behavioral Research*, *52*(6), 747–767. doi:10.1080/00273171.2017.1370364

Jonsen, I., Basson, M., Bestley, S., Bravington, M. V., Patterson, T. A., Pedersen, M. W., … Wotherspoon, S. J. (2013). State-space models for bio-loggers: A methodological road map. *Deep Sea Research Part II: Topical Studies in Oceanography*, *88–89*, 34–46. doi:10.1016/j.dsr2.2012.07.008

Katzner, T. E., Turk, P. J., Duerr, A. E., Miller, T. A., Lanzone, M. J., Cooper, J. L., … Lemaître, J. (2015). Use of multiple modes of flight subsidy by a soaring terrestrial bird, the golden eagle *Aquila chrysaetos*, when on migration. *Journal of the Royal Society Interface*, *12*, 20150530. doi:10.1098/rsif.2015.0530

Lanzone, M. J., Miller, T. A., Turk, P., Brandes, D., Halverson, C., Maisonneuve, C., … Katzner, T. (2012). Flight responses by a migratory soaring raptor to changing meteorological conditions. *Biology Letters*, *8*(5), 710–713. doi:10.1098/rsbl.2012.0359

Morales, J. M., Haydon, D. T., Frair, J., Holsinger, K. E., & Fryxell, J. M. (2004). Extracting more out of relocation data: building movement models as mixtures of random walks. *Ecology*, *85*(9), 2436–2445. doi:10.1890/03-0269

Murphy, M. A., Evans, J. S., & Storfer, A. (2010). Quantifying Bufo boreas connectivity in Yellowstone National Park with landscape genetics. *Ecology*, *91*(1), 252–61. doi:10.1890/08-0879.1

Péron, G., Fleming, C. H., Duriez, O., Fluhr, J., Itty, C., Lambertucci, S., … Calabrese, J. M. (2017). The energy landscape predicts flight height and wind turbine collision hazard in three species of large soaring raptor. *Journal of Applied Ecology*, *54*(6), 1895–1906. doi:10.1111/1365-2664.12909

Shirley, K. E., Small, D. S., Lynch, K. G., Maisto, S. A., & Oslin, D. W. (2010). Hidden Markov models for alcoholism treatment trial data. *The Annals of Applied Statistics*, *4*(1), 366–395. doi:10.1214/09-AOAS282